Supporting Information

Surface Functionalized Silica Nanoparticles for the Off-On Fluorogenic Detection of an Improvised Explosive, TATP, in a Vapour Flow.

José García-Calvo,[a] Patricia Calvo-Gredilla,[a] Marcos Ibáñez-Llorente,[a] Daisy C. Romero,[a] José V. Cuevas,[a] Gabriel García-Herbosa,[a] Manuel Avella,[b] Tomás Torroba,[a,*]

a.- Department of Chemistry, Faculty of Science, University of Burgos, 09001 Burgos, Spain.

b.- Advanced Microscopy Unit, Scientific Park Foundation, I+D Building, Miguel Delibes Campus, University of Valladolid, 47011 Valladolid, Spain. (ttorroba@ubu.es)

Index

1. SYNTHESIS OF PERYLENE DERIVATIVES:

General methods. The reactions performed with air sensitive reagents were conducted under dry nitrogen. The solvents were previously distilled under nitrogen over calcium hydride or sodium filaments. Column chromatography: SiO_2 (40-63 μm). TLC plates coated with SiO_2 60F254 were visualized by UV light. Melting points were determined in a Gallenkamp apparatus and are not corrected. FT-IR spectra were recorded on potassium bromide pellet with a JASCO FT/IR-4200. NMR spectra were recorded in Varian Mercury-300 and Varian Unity Inova-400 machines, in DMSO-d_6, $CDCl_3$, CD_3CN, CD_3OD. Chemical shifts are reported in ppm with respect to residual solvent protons, coupling constants ($J_{X\text{-}X'}$) are reported in Hz. MALDI-TOF mass spectra were measured on a MALDI-TOF Bruker Autoflex Mass Spectrometry instrument using DCTB and DIT matrixes. Quantitative UV-visible measures were performed with a Hitachi U-3900, in 1 cm UV cells at 25ºC. Fluorescence spectra were recorded in a Hitachi F-7000 FL spectrofluorometers, in 1 cm quartz cells at 25ºC. Quantum yield were measured with an integration sphere in a fluorometer Edinburgh Instruments FLS980. pH values were measured with a Metrohm 16 DMS Titrino pH meter with a combined glass electrode and a 3 M KCl solution as a liquid junction, calibrated with Radiometer Analytical SAS buffer solutions. Cyclic voltammetry experiments were registered in a Dropsens μStat 300 potenciostat with platinum bead working and platinum wire auxiliary electrodes and an Ag/AgCl electrode as reference. Scan rate 100 mV/s. Dry purified CH_2Cl_2 was used as solvent, and $[Bu_4N][PF_6]$ as supporting electrolyte. Ferrocene as internal reference was added at the end of each experiment.

Synthesis of *N*-(1-(1-adamantyl)ethyl)perylene-3,4-dicarboxylmonoimide (JG62)

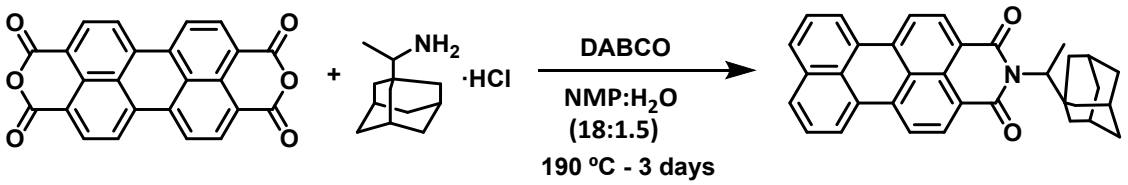

Figure S1: Synthesis of **JG62**

Perylene tetracarboxylic dianhydride (0.50 g, 1.28 mmol), DABCO (0.72 g, 6.4 mmol), and 1-(1-adamantyl)ethylamine hydrochloride (0.31 g, 1.43 mmol) were dissolved in *N*-methylpyrrolidone (NMP)/water 18.5 mL/1.5 mL and stirred in a high-pressure reactor at 190 ºC for 3 days. Then, the reaction mixture was poured into a 1M HCl solution in water (50 mL) and stirred for one hour. The resulting mixture was filtered under reduced pressure. The solid residue was purified by column chromatography (SiO_2, hexane to dichloromethane (DCM)), from which *N*-(1-(1-adamantyl)ethyl)perylene-3,4-dicarboxylmonoimide JG62 (303 mg, 49%) was obtained as an orange solid, m.p. 309–311 ºC. IR (KBr, cm^{-1}) 2903-2846, 1699 (C=O), 1650 (C=O), 1594, 1572, 1351, 1291, 1242, 1057, 1058, 810, 750. ^1H NMR ($CDCl_3$, 300 MHz) δ 8.48 (m, 2H, H_{Ar}), 8.30 (m, 4H, H_{Ar}), 7.83 (d, J = 7.9 Hz, 2H, H_{Ar}), 7.56 (t, 2H, J = 7.2 Hz, H_{Ar}), 5.10 (m, 1H, CH), 1.97 (s, 3H, 3xCH), 1.84-1.64 (m, 15H, 6xCH_2 + CH_3). ^{13}C NMR ($CDCl_3$, 75 MHz) δ (ppm) 165.8 (C=O), 165.1 (C=O), 136.9 (C_{Ar}), 134.5 (C_{Ar}), 132.1 ($C_{Ar}H$), 131.4 (C_{Ar}), 130.9(C_{Ar}), 129.9 (C_{Ar}), 129.5 ($C_{Ar}H$), 128.2 (C_{Ar}), 127.2 ($C_{Ar}H$), 126.8 (C_{Ar}), 123.7 ($C_{Ar}H$), 122.2 (C_{Ar}), 121.3 (C_{Ar}), 120.4 ($C_{Ar}H$), 58.3 (CH), 40.5 (CH_2), 38.3 (C_q), 37.2 (CH_2), 30.0 (CH_2), 13.4 (CH_3). HRMS (MALDI$^+$, DIT) m/z calcd. for $C_{34}H_{29}NO_2$ (M^+): 483.2193; found: 483.2224. UV-Vis (DCM), λ_{max} nm (log ε): 498 (4.5).

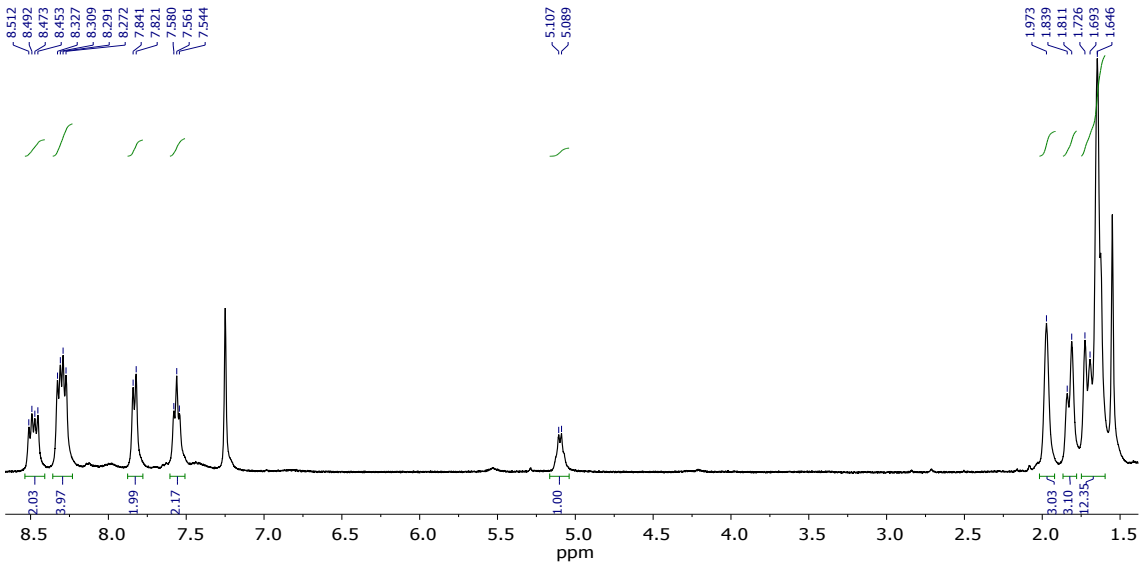

Figure S2: ^{1}H NMR ($CDCl_3$, 300 MHz) of JG62

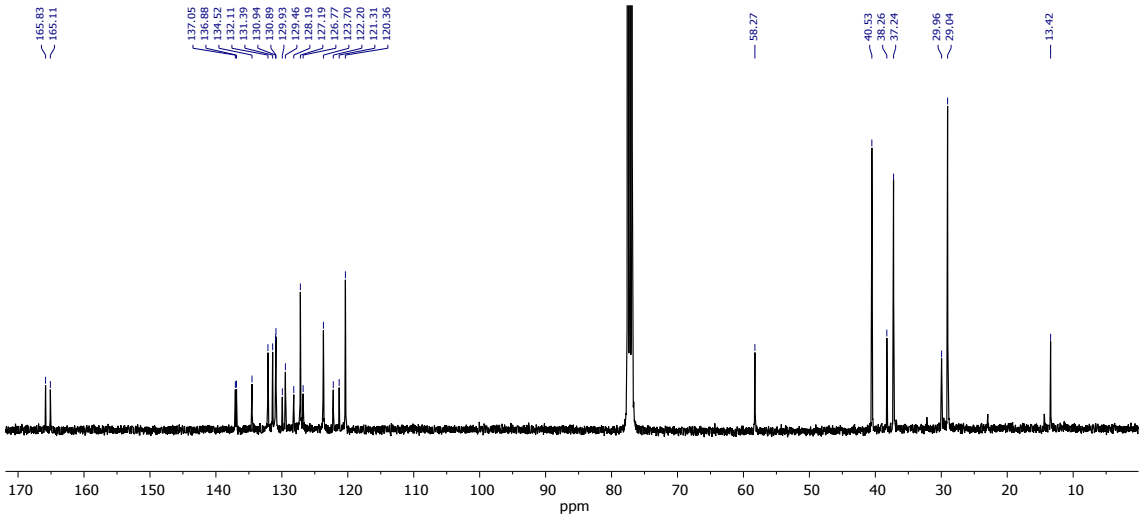

Figure S3: ^{13}C NMR ($CDCl_3$, 75 MHz) of JG62

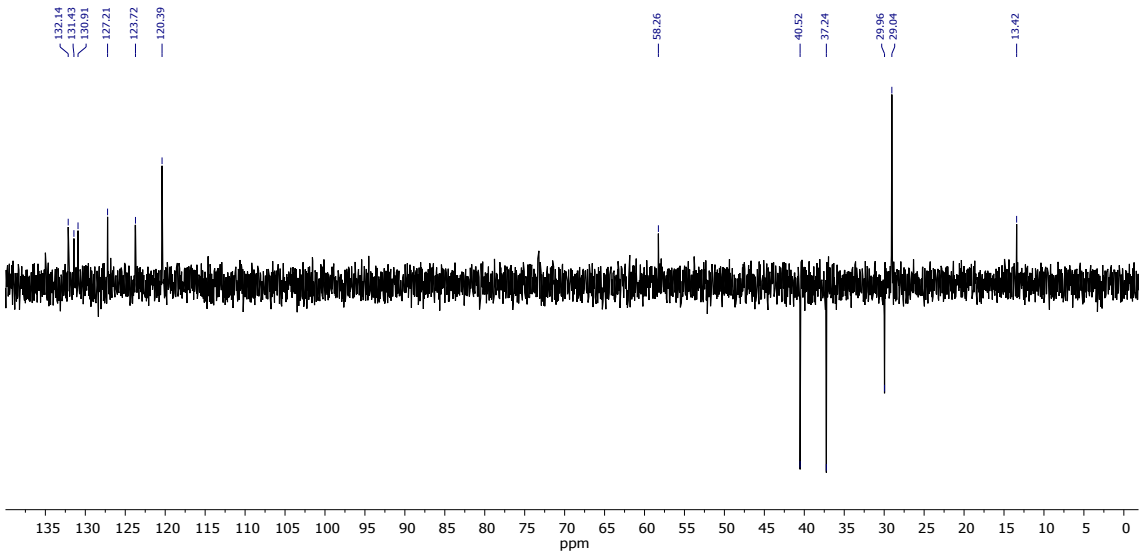

Figure S4: DEPT NMR ($CDCl_3$, 75 MHz) of JG62

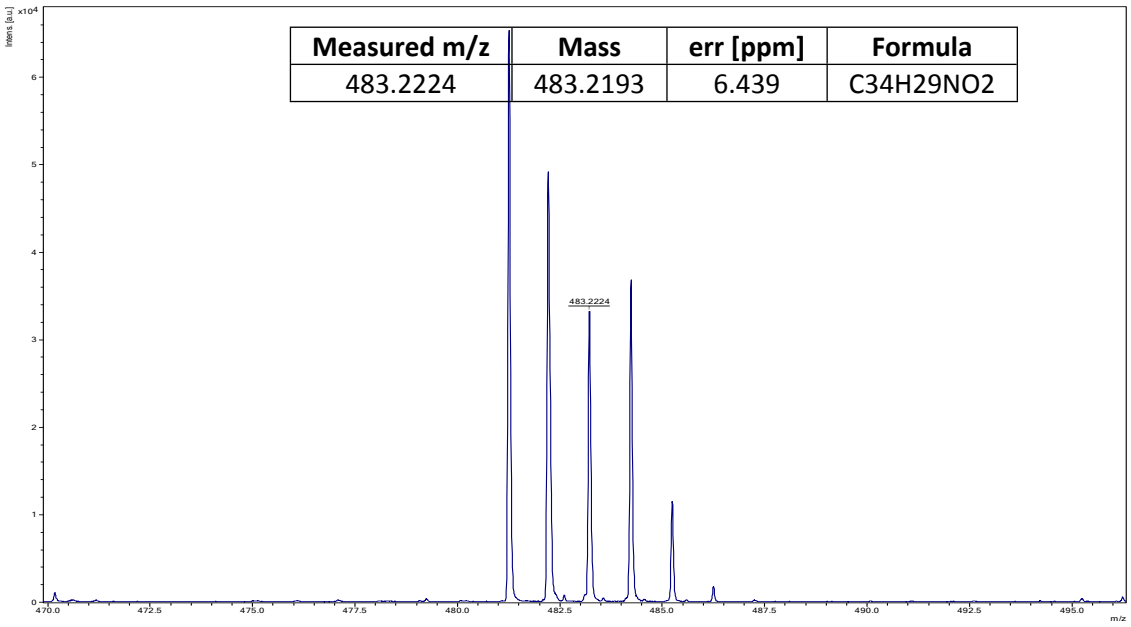

Figure S5: HRMS (MALDI$^+$, DIT) of JG62

Synthesis of *N*-(1-(1-adamantyl)ethyl)-8-bromoperylene-3,4-dicarboxylmonoimide (JG73)

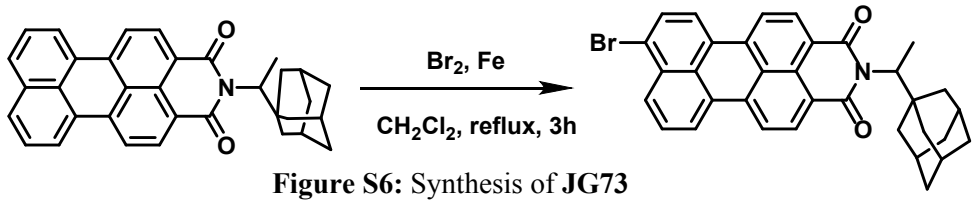

Figure S6: Synthesis of **JG73**

A solution of Br_2 (0.11 mL, 2.1 mmol) in DCM (2 mL) was added dropwise to a mixture of *N*-(1-(1-adamantyl)ethyl)perylene-3,4-dicarboxylmonoimide (JG62, 100 mg, 0.21 mmol) and Fe powder (2.3 mg, 20% mmol) in DCM (30 mL); afterwards, the resulting solution was refluxed for 3 hours. Then, a saturated solution of sodium sulfite or bisulfite in water was added to the reaction solution and the mixture was extracted 3 times with DCM (100 mL); the combined organic extracts were washed with 20 mL of water, dried (Na_2SO_4) and the solvent evaporated under reduced pressure. The solid residue was purified by column chromatography (SiO_2, DCM), from which *N*-(1-(1-adamantyl)ethyl)perylene-8-bromo-3,4-dicarboxylmonoimide JG73 (117 mg, 89%) was obtained as a red solid, m.p. 338–339 ^oC. IR (KBr, cm^{-1}) 3090, 3072, 2905, 2847, 1692 (C=O), 1658 (C=O), 1594, 1565, 1454, 1410, 1374, 1347, 1313, 1288, 1247, 1204, 1179, 1114, 1099, 1058, 1036, 1017 (C-Br), 910, 841, 822, 803, 754, 684. ^1H NMR (300 MHz, $CDCl_3$) δ 8.62–8.50 (m, 2H, H_{Ar}), 8.37 (ddd, J = 27.5 Hz, J = 16.8 Hz, J = 8.0 Hz, 4H, H_{Ar}), 8.19 (d, J = 8.2 Hz, 1H, H_{Ar}), 7.88 (d, J = 8.1 Hz, 1H, H_{Ar}), 7.70 (t, J = 8.0 Hz, 1H, H_{Ar}), 5.10 (q, J = 7.3 Hz, 1H, CH), 1.98 (s, 3H, 3xCH), 1.80 (m, 3H, 1.5xCH_2), 1.66 (m, 12H, 4.5xCH_2 + CH_3). ^{13}C NMR (100 MHz, $CDCl_3$) δ 165.6 (C=O), 164.9 (C=O), 136.3 (C_{Ar}), 133.2 (C_{Ar}), 132.2 ($C_{Ar}H$), 132.1 ($C_{Ar}H$), 131.5 ($C_{Ar}H$), 131.4 ($C_{Ar}H$), 130.0 (C_{Ar}), 130.0 (C_{Ar}), 129.9 (C_{Ar}), 129.5 ($C_{Ar}H$), 128.3 ($C_{Ar}H$), 126.4 (C_{Ar}), 124.3 (C_{Ar}), 123.7 (C_{Ar}), 123.7 ($C_{Ar}H$), 120.9 ($C_{Ar}H$), 120.6 ($C_{Ar}H$), 58.3 (CH), 40.5 (CH_2), 38.2 (C_q), 37.2 (CH_2), 29.0 (CH_2), 13.3 (CH_3). HRMS

(MALDI$^+$, DCTB) m/z calcd for $C_{34}H_{28}BrNO_2$ (M^+): 561.1298; found: 561.1287. UV-Vis (DCM), λ nm (log ε): 499 (4.5).

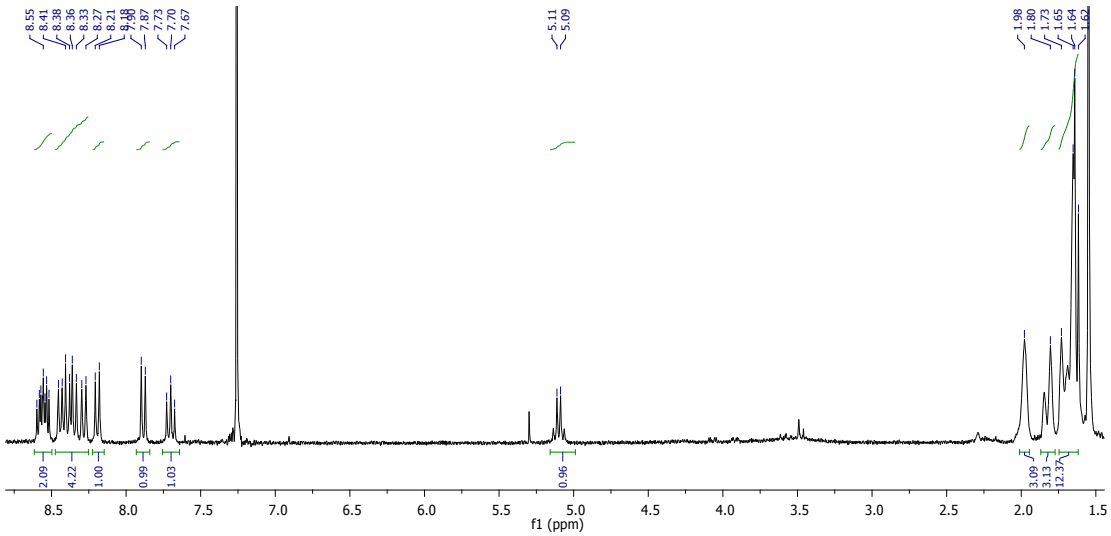

Figure S7: ^{1}H NMR ($CDCl_3$, 300 MHz) of JG73

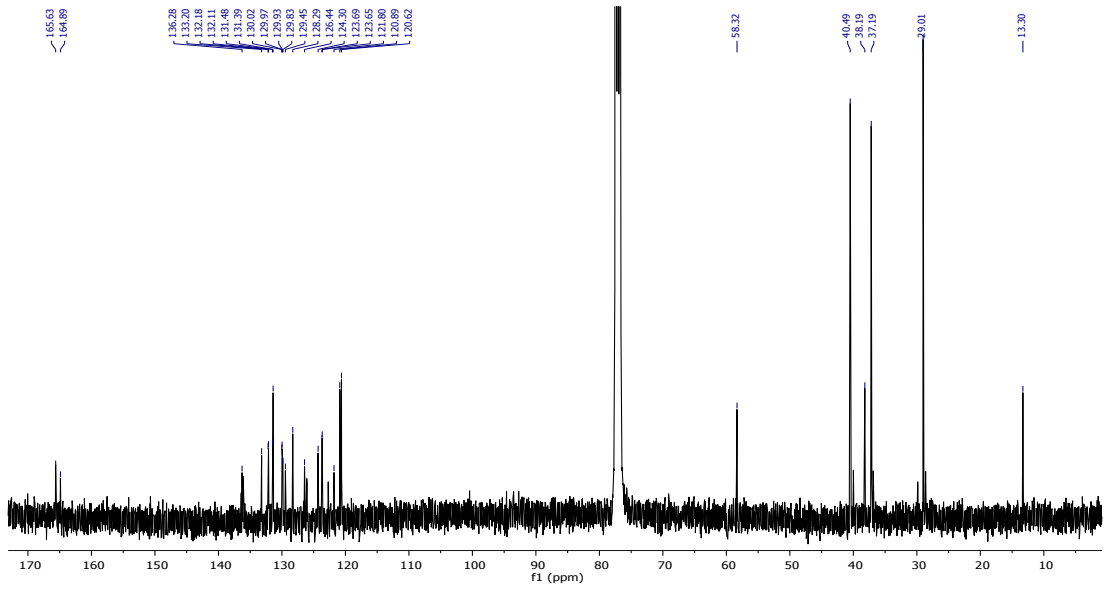

Figure S8: ^{13}C NMR ($CDCl_3$, 100 MHz) of JG73

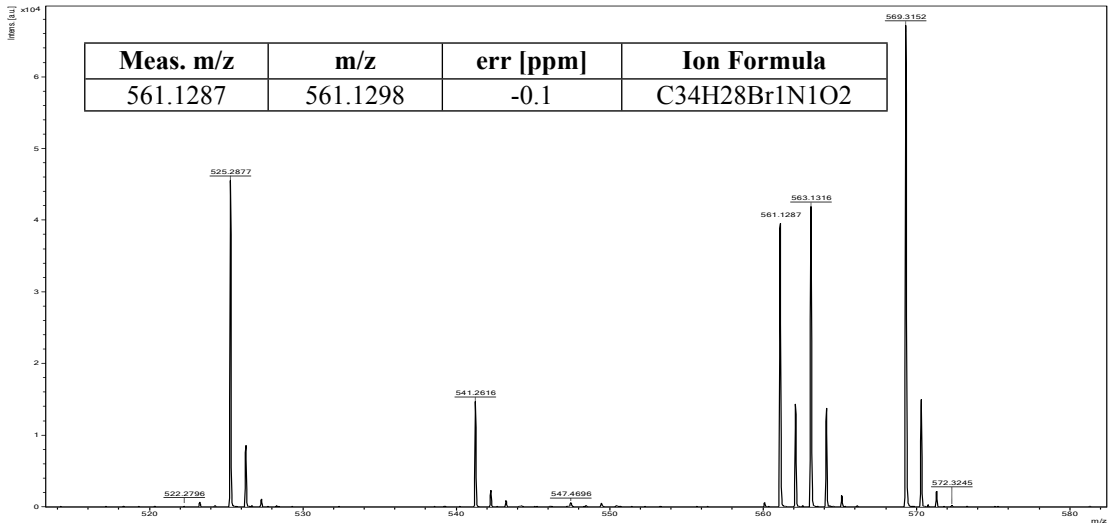

Figure S9: HRMS (MALDI$^+$, DCTB) of JG73

Synthesis of *N*-[1-(1-adamantyl)ethyl] 8-[2-(*N*-Boc-piperazin-1-yl)pyrid-5-yl]perylene-3,4-dicarboxylmonoimide (JG125)

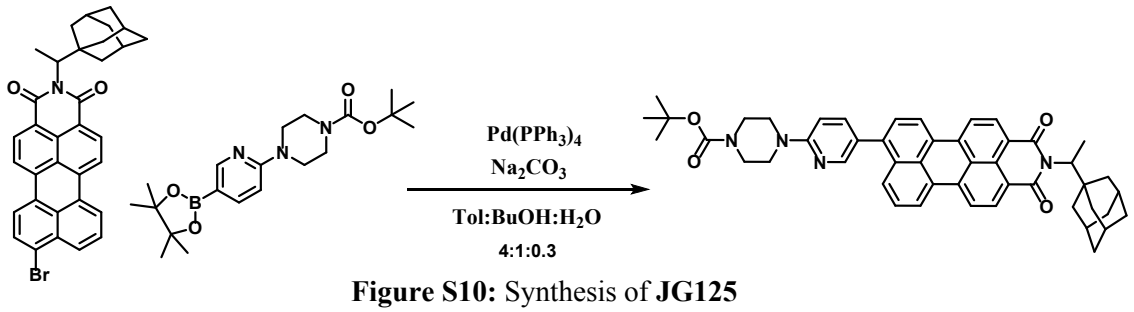

Figure S10: Synthesis of **JG125**

In a 100 mL Schlenk, provided with magnetic stirrer and cooler, 150 mg (0.27 mmol) of N-(1-(1-adamantyl)ethyl) perylene-8-bromo-3,4-dicarboxylmonoimide, **JG73**, 113 mg (0.29 mmol) of 2-(4-*N*-Boc-piperazin-1-yl)pyrid-5-yl boronic acid, pinacol ester, 143 mg (1.35 mmol) of Na_2CO_3 and 15 mg (0.014 mmol) $Pd(PPh_3)_4$ were added under nitrogen atmosphere. Then, they were solved into the mixture Tol:BuOH:H_2O (8:2:0.6 ml) and heated under reflux for 24 hours. After that, 100 mL of water were added to the mixture and extracted with CH_2Cl_2 (3 x 75 mL). The combined organic extracts were dried (Na_2SO_4) and the solvent was evaporated. As a result, the product was obtained and purified by column chromatography DCM:MeOH 4% v/v, obtaining **JG125**, 138 mg, as a purple solid, 69% yield. m.p. 304-305 ºC, decomposition. IR (KBr, cm^{-1}) 2958 - 2923 (C_{Ar}-H), 2853 (C-H), 1738 (C=O), 1651 (C=O), 1598 (C_{Ar}-C_{Ar}), 1462 (C-O), 1393, 1285, 1240, 1173(C-N), 1361, 1121, 1072, 1055, 936. ^{1}HNMR (300 MHz, $CDCl_3$) δ 8.33 (s, 1H, N=CH (pyr)), 8.26 – 8.18 (m, 2H, H_{Ar}), 8.00 (t, *J* = 7.2 Hz, 2H, H_{Ar}), 7.86 (dd, *J* = 13.6, 6.9 Hz, 3H, H_{Ar}), 7.7 (m, 1H, CH-C=N), 7.40 – 7.23 (m, 2H, H_{Ar}), 6.84 (d, *J* = 8.8 Hz, 1H, H_{Ar}), 5.07 (q, *J* = 7.0 Hz, 1H, NC**H**CH_3), 3.65 (m, 8H, 2xCH_2), 1.97 (s, 3H, 1.5xCH_2), 1.80 (m, 3H, 1.5xCH_2), 1.80-1.61 (m, 12H, 4.5xCH_2+CH_3), 1.52 (s, 9H, $C(CH_3)_3$). ^{13}C NMR (100 MHz, $CDCl_3$) δ 165.5 (C=O), 164.9 (C=O), 158.8 (N-C=N), 155.1 (O-C=O), 148.5 (C_{Ar}H), 139.4 (C_{Ar}), 131.6 (C_{Ar}), 130.9 (C_{Ar}H), 128.2 (C_{Ar}), 125.2 (C_{Ar}H), 124.2 (C_{Ar}H), 123.5 (C_{Ar}H), 120.0 (C_{Ar}H), 119.7 (C_{Ar}H), 106.8 (C_{Ar}H), 80.3 ($C(CH_3)_3$), 57.9 (NCH), 45.2 (NCH_2), 37.2 (NCH_2), 40.5 (CH_2 adam), 38.2 (CH_2 adam), 28.7 (CH_2 + CH_3), 13.4 (CH_3). HRMS (MALDI$^-$, DCTB) m/z calcd for $C_{48}H_{48}N_4O_4$: 744.3670 (M$^-$, DCTB); found: 744.4270. UV-Vis (DCM), λ nm (log ε): 511 (4.6).

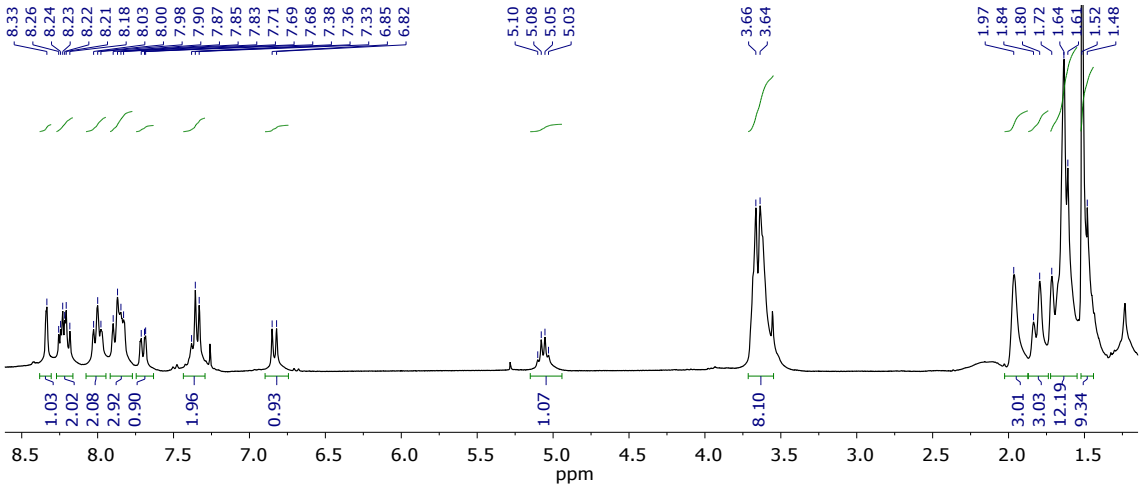

Figure S11: ^{1}H NMR ($CDCl_3$, 300 MHz) of JG125

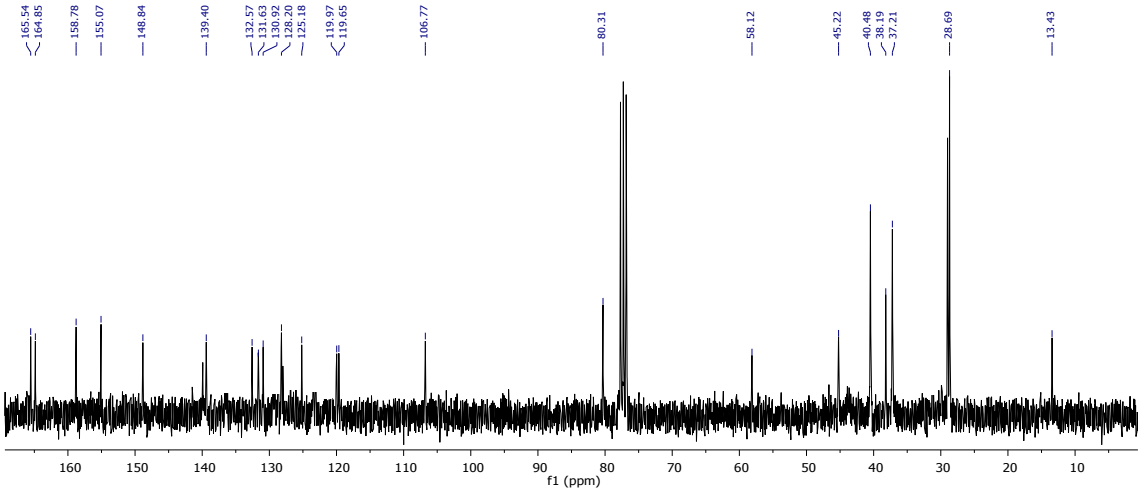

Figure S12: ^{13}C NMR ($CDCl_3$, 300 MHz) of JG125

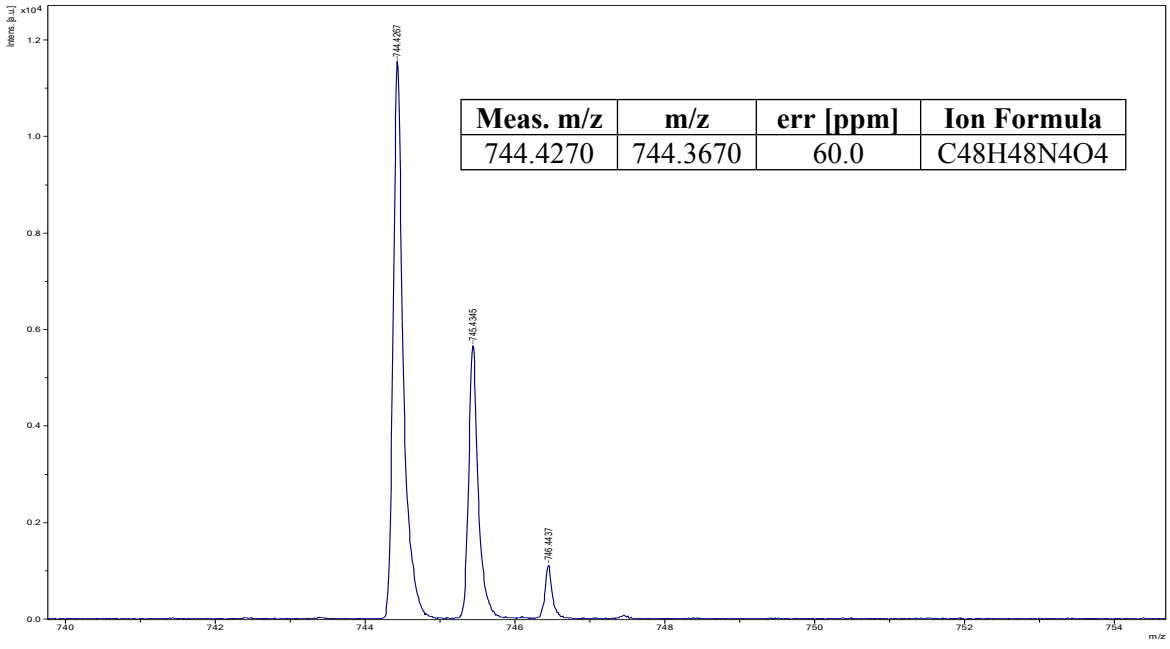

Meas. m/z	m/z	err [ppm]	Ion Formula
744.4270	744.3670	60.0	C48H48N4O4

Figure S13: HRMS (MALDI^{-}, DCTB) of JG125

Synthesis of *N*-[2-(1-adamantyl)ethyl] 8-[2-(piperazin-1-yl)pyrid-5-yl]perylene-3,4-dicarboxylmonoimide (JG125d)

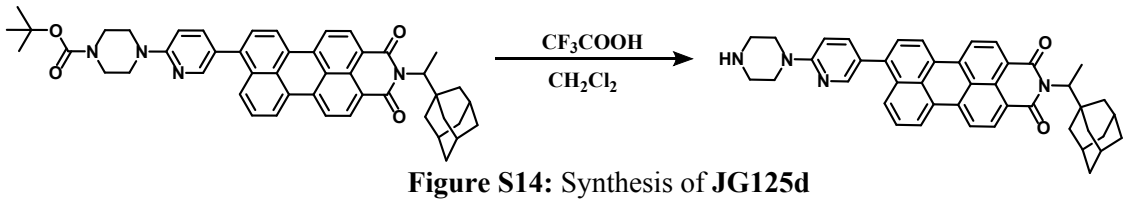

Figure S14: Synthesis of **JG125d**

150 mg (0.21 mmol) of the boc protected product **JG125** were dissolved in CH_2Cl_2 (20 mL). Then, trifluoroacetic acid (5 mL, ρ= 1.489 g/mL, 65.3 mmol) was added dropwise into the flask with the solution under stirring. The resulting mixture was stirred at room temperature for 30 minutes. 50 mL of water and a 5% NaOH basic solution were added until reaching pH=10. After that, an extraction was carried out with CH_2Cl_2:Water (4 x 50 mL CH_2Cl_2). The combined organic extracts were dried using Na_2SO_4, filtered and the solvent evaporated under reduced pressure to get the product as 129 mg of a purple-red solid, 95% yield. m.p. 299-300 ^oC, decomposition. IR (KBr, cm^{-1}) 3422 (N-H), 2923 (C_{Ar}-H), 2850 (C-H), 1696 (C=O), 1651.01 (C=O), 1595 (C_{Ar}-C_{Ar}), 1494 (C-O), 1382, 1246, 1201, 1177 (C-N), 1351, 1153, 1100, 1038, 1010, 940. ^1H NMR (300 MHz, $CDCl_3$) δ 8.48 (m, 2H, H_{Ar}), 8.37-8.24 (m, 5H, H_{Ar}), 7.98 (m, *J* = 7.4 Hz, 1H, H_{Ar}), 7.70 (dd, *J* = 8.7, 2.5 Hz, 3H, H_{Ar}), 7.52-7.48 (m, 2H, H_{Ar}), 6.83 (d, *J* = 8.8 Hz, 1H, H_{Ar}), 5.10 (q, *J* = 7.2 Hz, 1H, NCH), 3.65 (m, 4 H, 2xCH_2), 3.58 (m, 1H br, NH), 3.06 (m, 4H, 2xCH_2), 1.98 (s, 3H, 1.5xCH_2), 1.83 (m, 3H, 1.5xCH_2), 1.74-1.62 (m, 12H, 4.5xCH_2+CH_3). ^{13}C NMR (100 MHz, $CDCl_3$) δ 165.5 (C=O), 164.8 (C=O), 158.9 (N-C=N), 148.6 ($C_{Ar}H$), 139.0 (C_{Ar}), 131.8 (C_{Ar}), 131.1 ($C_{Ar}H$), 129.7 (C_{Ar}), 129.4 ($C_{Ar}H$), 128.4 ($C_{Ar}H$), 128.0 ($C_{Ar}H$), 126.9 ($C_{Ar}H$), 126.4 ($C_{Ar}H$), 123.6 ($C_{Ar}H$), 123.3 ($C_{Ar}H$), 120.1 ($C_{Ar}H$), 119.8 ($C_{Ar}H$), 106.4 ($C_{pyr}H$), 58.0 (NCH), 45.9 (CH_2), 40.3 (CH_2), 38.0 (CH_2), 37.0 (CH_2 adam), 29.7 (CH_2), 28.8 (CH), 13.1 (CH_3). HRMS (MALDI$^-$, DIT) m/z calcd for $C_{43}H_{40}N_4O_2$: 644.3146 (M^-); found: 644.3056. UV-Vis (DCM), λ nm (log ε): 511 (4.3).

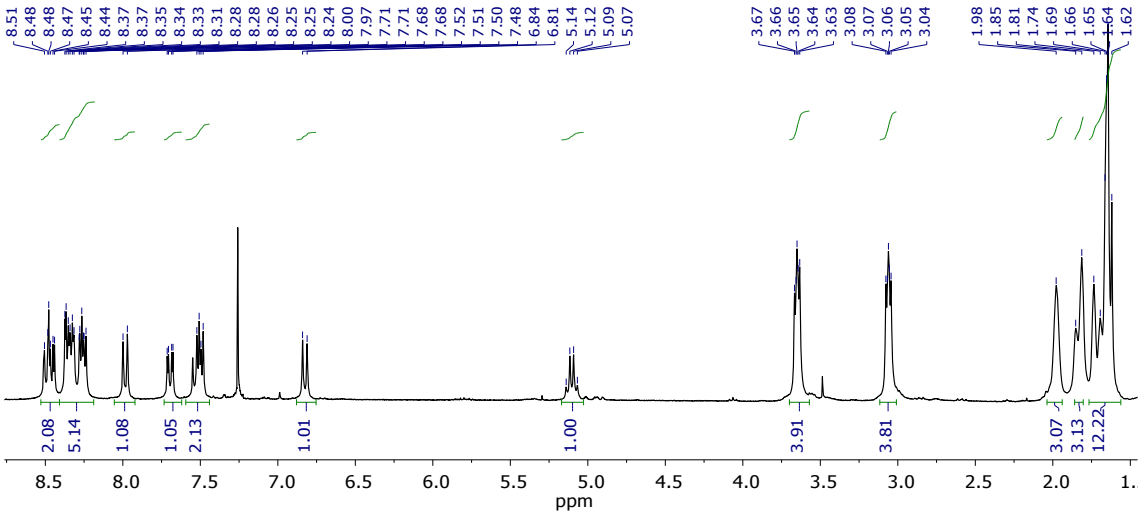

Figure S15: ^1H NMR ($CDCl_3$, 300 MHz) of JG125d

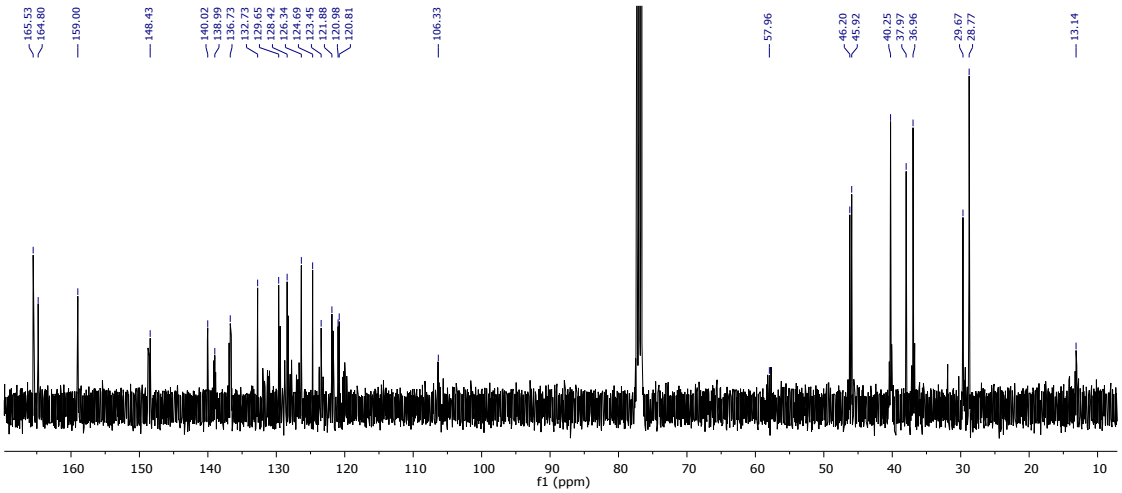

Figure S16: ^{13}C NMR ($CDCl_3$, 100 MHz) of JG125d

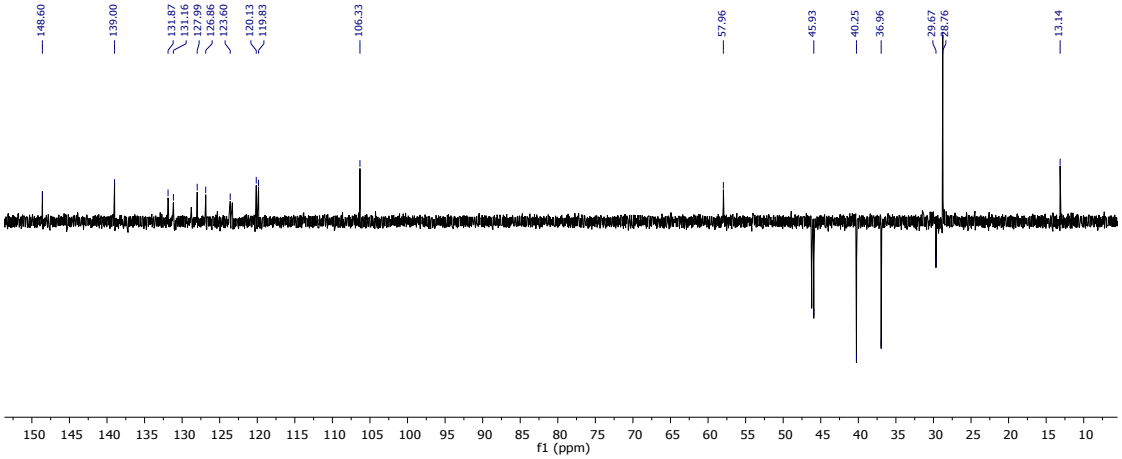

Figure S17: DEPT NMR ($CDCl_3$, 100 MHz) of JG125d

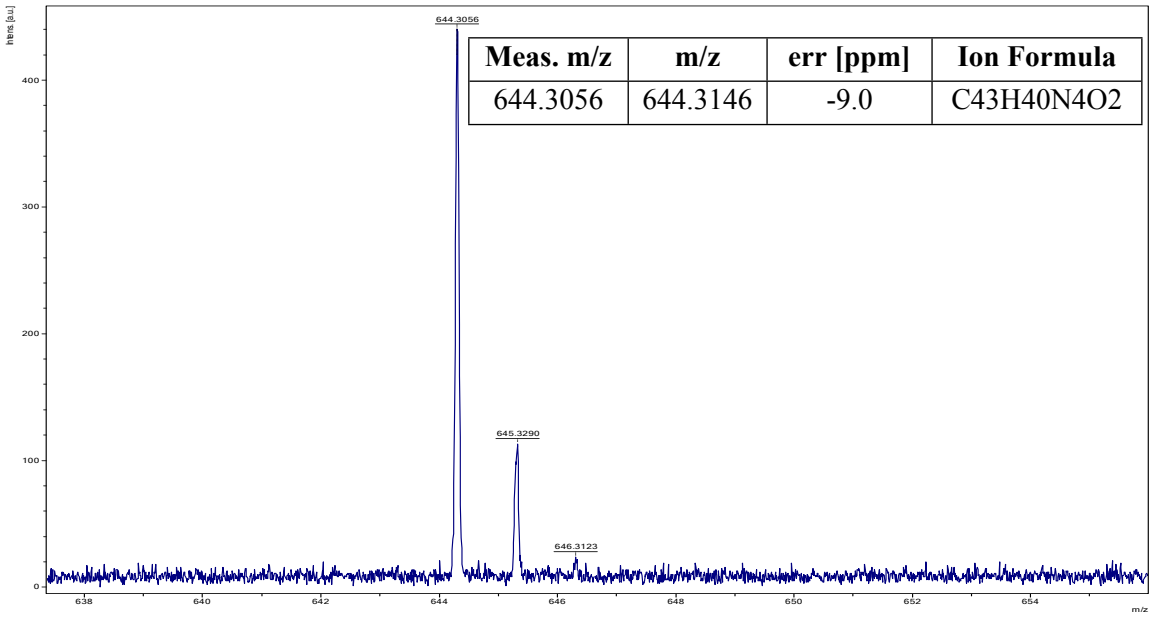

Meas. m/z	m/z	err [ppm]	Ion Formula
644.3056	644.3146	-9.0	C43H40N4O2

Figure S18: HRMS (MALDI$^-$, DIT) of JG125d

Synthesis of *N*,*N*'-Dicyclohexyl-1-[2-(*N*-Boc-piperazin-1-yl)pyrid-5-yl]perylene-3,4:9,10-tetracarboxydiimide (PC63).

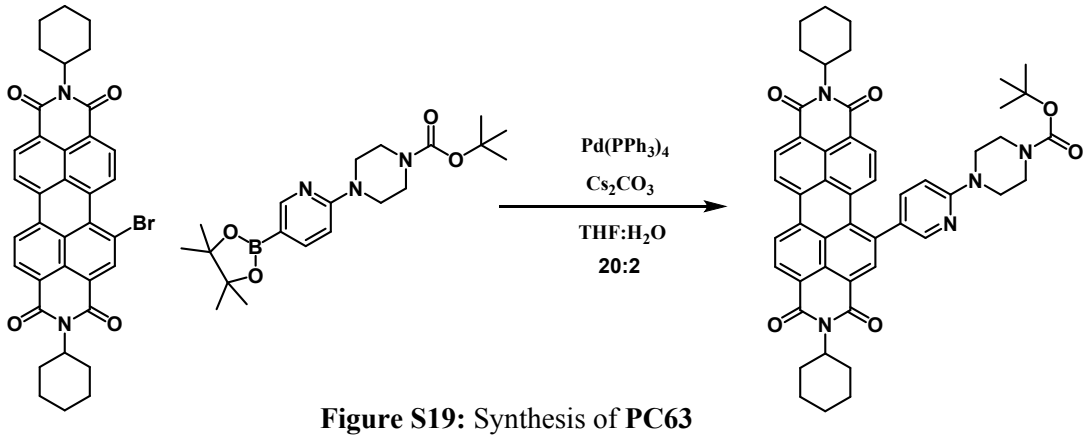

Figure S19: Synthesis of **PC63**

N,*N*'-Dicyclohexyl-1-bromoperylene-3,4:9,10-tetracarboxydiimide (100 mg, 0.16 mmol) was placed in a Schlenk flask under nitrogen atmosphere, then THF:H_2O (20:2 ml), and 15 mg (0.014 mmol) of tetrakis(triphenylphosphine)palladium(0) were added. The mixture was stirred for 5 minutes. After that time 2-(*N*-Boc-piperazin-1-yl)pyrid-5-yl boronic acid, pinacol ester, (67 mg, 0.17 mmol) and caesium carbonate (168 mg, 0.47 mmol) were added. After 24 hours under reflux, the crude was extracted with dichloromethane (4 × 50 mL CH_2Cl_2) and dried with Na_2SO_4. Finally, the crude product was purified by column chromatography (silica gel, CH_2Cl_2:CH_3CN) and perylene bisimide **PC63** was obtained as a purple solid in 66 % yield (85 mg, 0.104 mmol). m.p,: 214–216 ºC. FT-IR (KBr, cm^{-1}): 2926 (C-H), 2855 (C-H), 1698 (C=O), 1658 (C=O), 1590 (CAr-CAr), 1493, 1454 (CH2), 1405 (C-N), 1331, 1235, 1164, 1118, 1022, 860, 811, 749 (fingerprint region). ^{1}H NMR (300 MHz, $CDCl_3$) δ: 8.65 – 8.50 (m, 5H, H_{Ar}), 8.49 (s, 1H, H_{Ar}), 8.31 (d, J = 2.5 Hz, 1H, H_{Ar}), 8.20 (d, J = 8.2 Hz, 1H, H_{Ar}), 8.06 (d, J = 8.2 Hz, 1H, H_{Ar}), 7.52 (dd, J = 8.8, 2.5 Hz, 1H, H_{Ar}), 6.72 (d, J = 8.9 Hz, 1H, H_{Ar}), 5.08 – 4.96 (m, 2H, N-CH), 3.66 – 3.63 (m, 8H, CH_2), 2.59 – 2.51 (m, 4H, CH_2), 1.91 (m, 4H, CH_2), 1.74 (m, 6H, CH_2), 1.52 (s, 9H, CH_3), 1.48 – 1.30 (m, 6H, CH_2). ^{13}CNMR (101 MHz, $CDCl_3$) δ 164.0 (C=O), 163.9 (C=O), 163.8 (C=O), 163.7 (C=O), 158.6 (C_{Ar}-N), 154.9 ($COOC(CH_3)_3$), 147.8 (CH), 138.6 (C_{Ar}), 138.1 ($C_{Ar}H$), 136.0 ($C_{Ar}H$), 134.8 (C_{Ar}), 134.5 (C_{Ar}), 134.3 (C_{Ar}), 132.2 (C_{Ar}), 131.2 ($C_{Ar}H$), 131.0 ($C_{Ar}H$), 130.6 ($C_{Ar}H$), 130.2 ($C_{Ar}H$), 129.3 (CH), 129.0 (C_{Ar}), 128.2 (C_{Ar}), 128.1 (C_{Ar}), 127.6 (C_{Ar}), 127.5 (C_{Ar}), 123.7 (CH), 123.6 (C_{Ar}), 123.1 (C_{Ar}), 122.9 (C_{Ar}), 122.7 (CH), 122.5 (C_{Ar}), 107.7 (CH), 80.3 (C_q), 54.2 (CH), 54.1 (CH), 44.9 (CH_2), 29.3 (CH_2), 29.2 (CH_2), 28.6 (CH_3), 26.7 (CH_2), 26.7 (CH_2), 25.6 (CH_2). HRMS (MALDI$^-$, DIT): m/z calcd. for $C_{50}H_{49}N_5O_6$ ($[M]^-$): 815.3677; found: 815.3680. UV-Vis (DCM), λ nm (log ε): 484 (4.4), 521 (4.4).

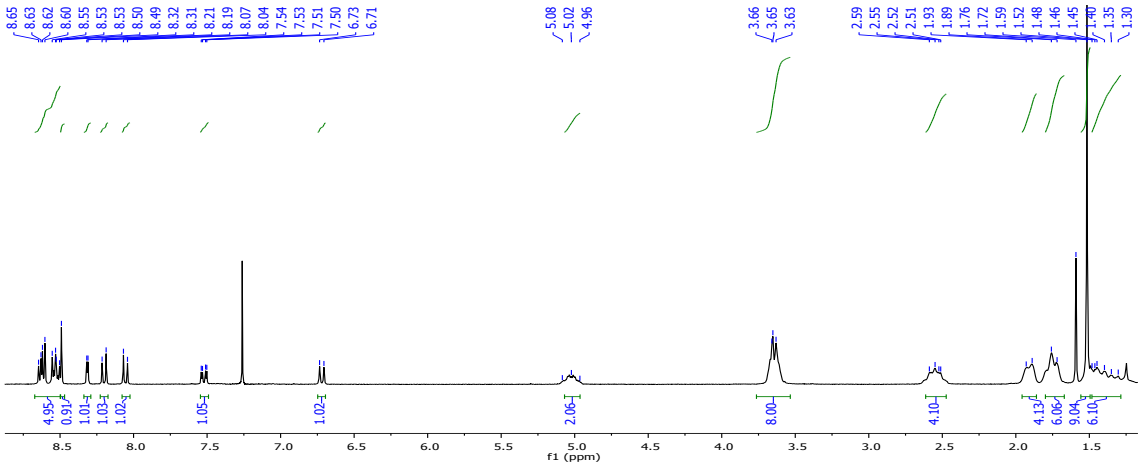

Figure S20: ^{1}H NMR ($CDCl_3$, 300 MHz) of PC63

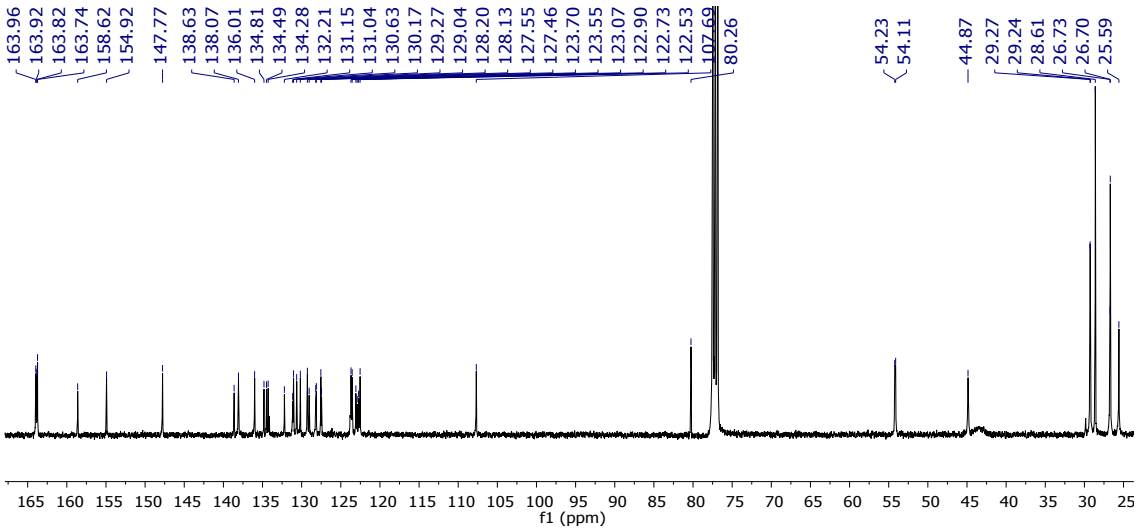

Figure S21: ^{13}C NMR ($CDCl_3$, 100 MHz) of PC63

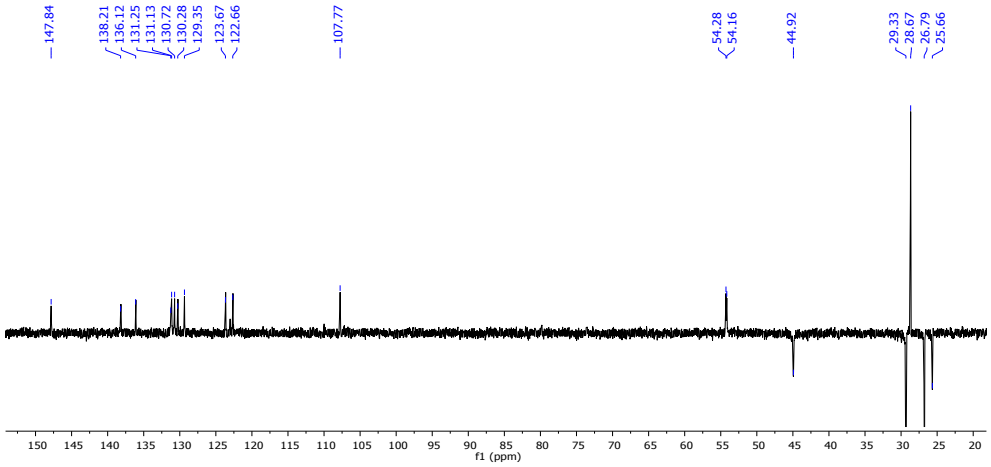

Figure S22: DEPT NMR ($CDCl_3$, 100 MHz) of PC63

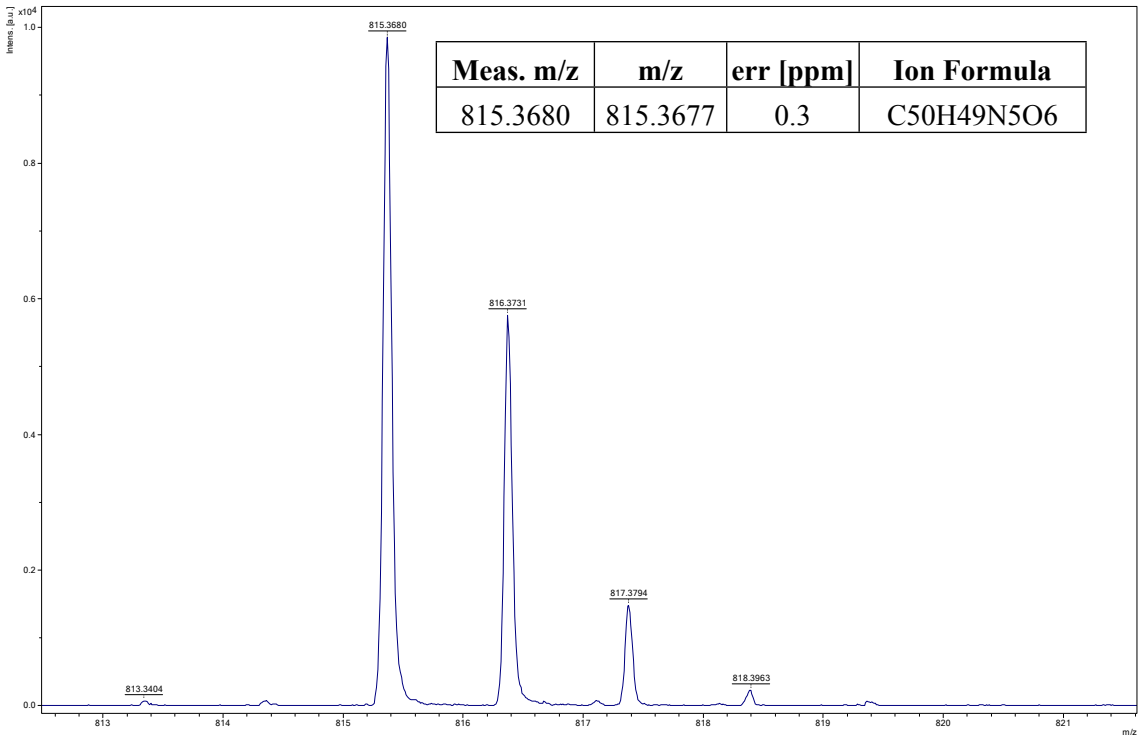

Meas. m/z	m/z	err [ppm]	Ion Formula
815.3680	815.3677	0.3	C50H49N5O6

Figure S23: HRMS (MALDI$^-$, DIT) of PC63

Synthesis of *N*,*N*'-Dicyclohexyl-1-[2-(piperazin-1-yl)pyrid-5-yl]perylene-3,4:9,10-tetracarboxydiimide (PC63d).

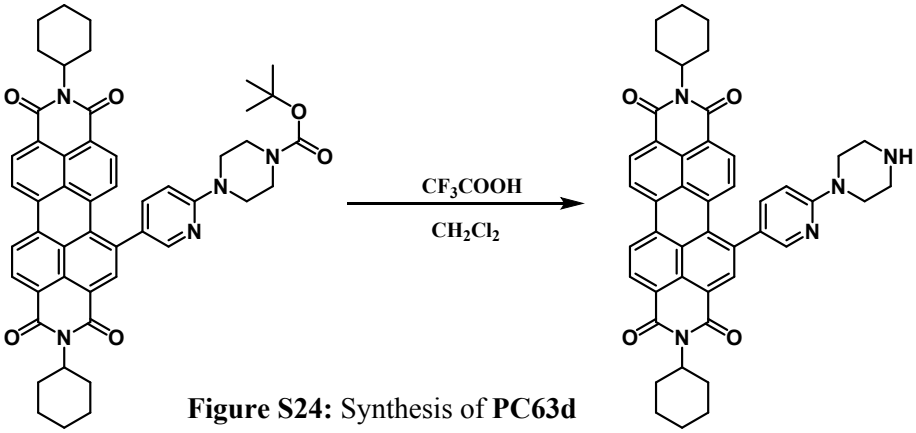

Figure S24: Synthesis of **PC63d**

20 mg of **PC63** (0.025 mmol) were dissolved in CH_2Cl_2 (5 mL). Then, trifluoroacetic acid (1 mL, ρ= 1.489 g/mL, 13.1 mmol) was added dropwise under stirring. The resulting mixture was stirred at room temperature for 30 minutes. Afterwards, 10 mL of water and a 5% NaOH basic solution were added until reaching pH=10. Then, an extraction was performed with CH_2Cl_2:Water (4 x 20 mL). The combined organic extracts were dried using Na_2SO_4, filtered and the solvent evaporated under reduced pressure to get the product, 17 mg, as a purple-red solid, 95% yield, m.p. 220-221 ^oC. IR (KBr, cm^{-1}) 3439 (N-H), 2924 (C_{Ar}-H), 2852 (C-H), 1693 (C=O Imide), 1655 (C=O), 1590 (C_{Ar}-C_{Ar}), 1496 (C-O), 1455, 1402, 1333 (C-N), 1240, 1019, 1010, 808, 749. ^1H NMR (300 MHz, $CDCl_3$) δ 8.63 – 8.57 (m, 2H, H_{Ar}), 8.52 – 8.46 (m, 3H, H_{Ar}), 8.31 (d, J = 2.6 Hz, 1H, H_{Ar}), 8.20 (d, J = 8.2 Hz, 1H, H_{Ar}), 8.05 (d, J = 8.4 Hz, 1H, H_{Ar}),

7.49 (dd, J = 8.8, J = 2.5 Hz, 1H, H_{Ar}), 6.71 (d, J = 9.0 Hz, 1H, H_{Ar}), 5.05 – 5.01 (m, 2H, CH), 3.66 (t, J = 5.0 Hz, 4H, CH_2), 3.06 (t, J = 5.0 Hz, 4H, CH_2), 2.85 (m, 1H, br, NH), 2.59 – 2.52 (m, 4H, CH_2), 1.89 (d, 4H, CH_2), 1.76 (m, 6H, CH_2), 1.49 – 1.37 (m, 4H, CH_2). ^{13}C NMR (75 MHz, $CDCl_3$) δ 164.1 (C=O), 163.9 (C=O), 163.9 (C=O), 163.7 (C=O), 159.0 (C_{Ar}), 147.8 (C_{Ar}), 138.9 (C), 138.0 (C), 136.2 (C), 135.0 (C), 134.6 (C), 134.5 (C), 132.3 (C), 131.2 (C), 130.7 (C), 130.3 (C), 129.9 (C), 129.3 (C), 128.3 (C), 127.6 (C), 127.3 (C), 123.9 (C), 123.8 (C), 123.7 (C), 123.1 (C), 122.8 (C), 122.6 (C), 107.6 (C), 54.2 (CH), 46.0 (CH_2), 45.9 (CH_2), 32.1 (CH_2), 29.9 (CH_2), 29.3 (CH_2), 26.7 (CH_2), 25.6 (CH_2). HRMS (MALDI$^+$, DCTB): m/z calcd. for $C_{45}H_{41}N_5O_4$ ([M+H]$^+$): 716.3231; found: 716.3255.

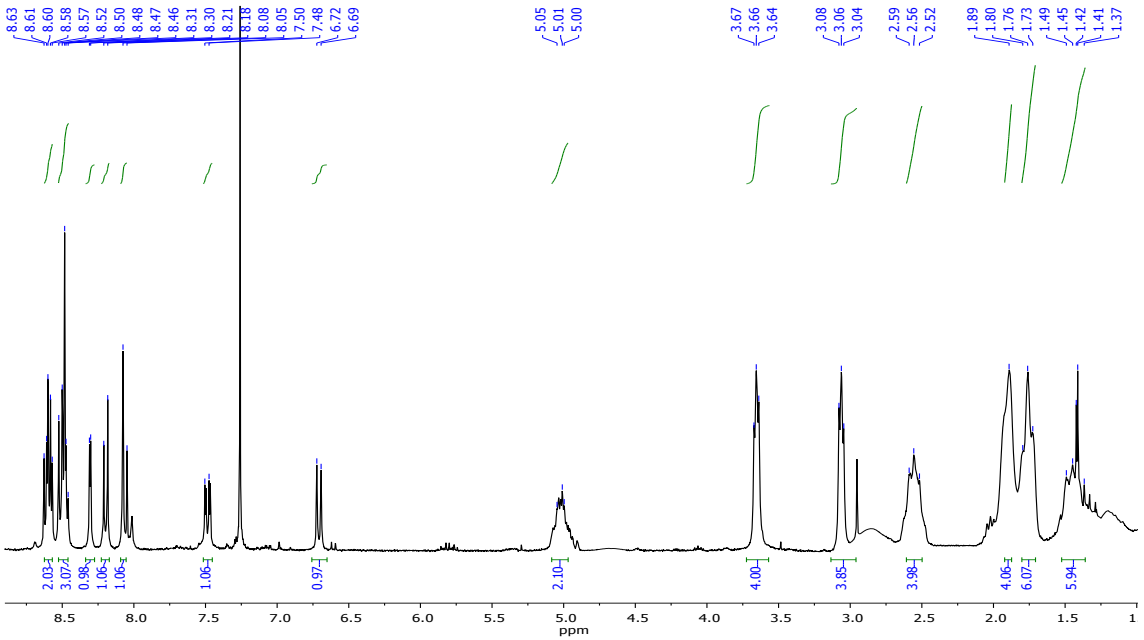

Figure S25: ^{1}H NMR ($CDCl_3$, 300 MHz) of PC63d

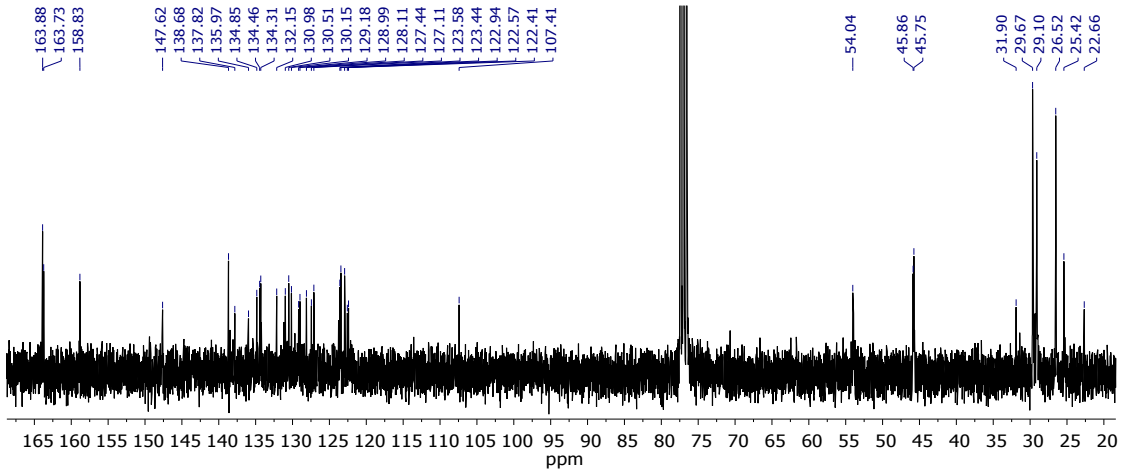

Figure S26: ^{13}C NMR ($CDCl_3$, 75 MHz) of PC63d

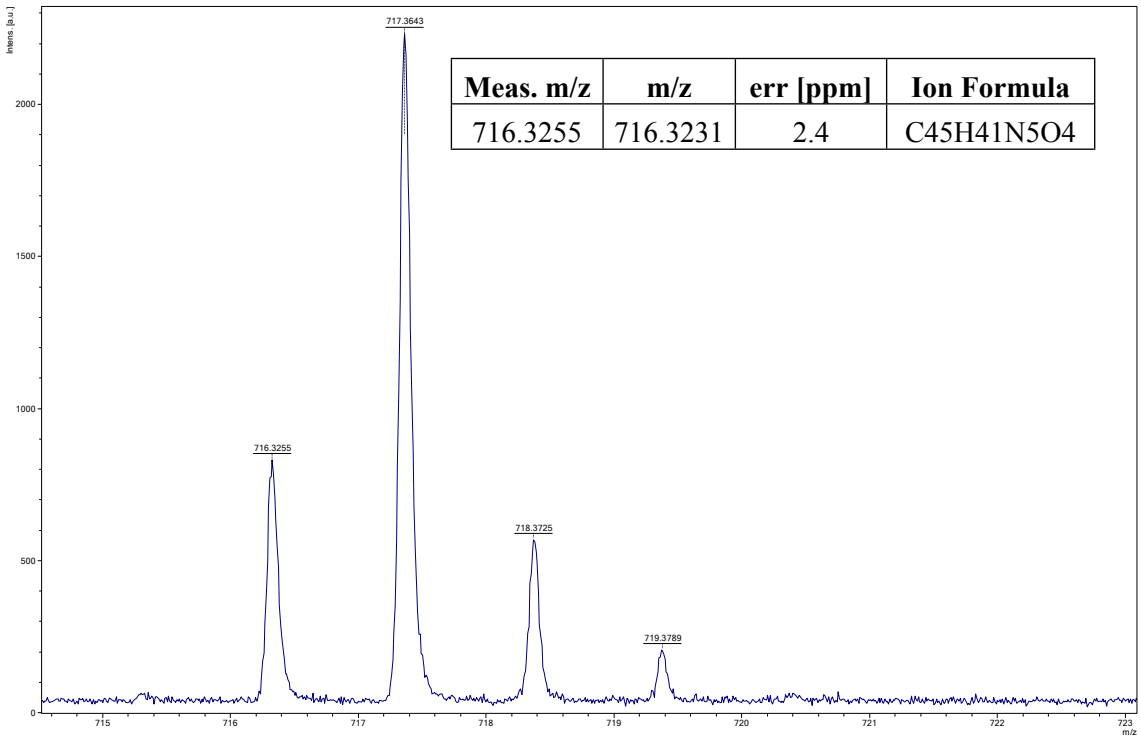

Meas. m/z	m/z	err [ppm]	Ion Formula
716.3255	716.3231	2.4	C45H41N5O4

Figure S27: HRMS (MALDI$^+$, DCTB) of PC63d

2. PREPARATION AND CHARACTERIZATION OF SILICA SUBSTITUTED NANOPARTICLES

2.1. Synthesis of triethoxysilyl perylene derivatives:

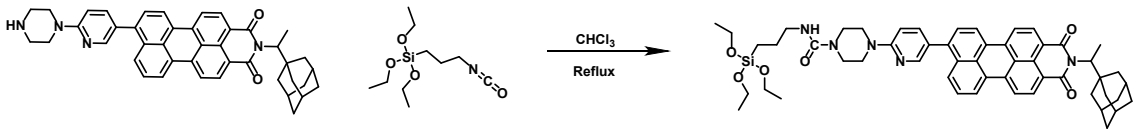

Figure S28. Synthesis of the triethoxysilyl derivative, JG131 from JG125-deprotected

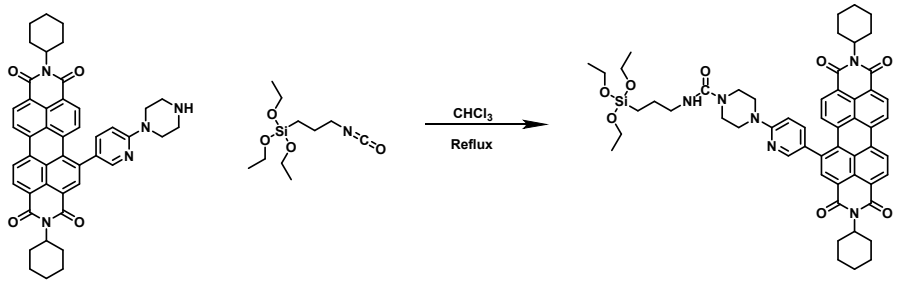

Figure S29. Synthesis of the triethoxysilyl derivative of JG135 from PC63-deprotected

The corresponding perylene imide (20 mg, 0.03 mmol) was dissolved in 5 ml of $CHCl_3$. Then, triethoxy(3-isocyanatopropyl)silane (8 mg, 0.03 mmol) was added to the solution and stirred under reflux for 24 hours. The resulting product was checked by ^{1}HNMR and introduced to the next reaction without further purification.

2.2. Synthesis of silica materials with supported perylene derivatives:

Silica 10-20 nm Sigma Aldrich 99.5 % and TLC plates Merck Aluminium sheets 5x10 cm Silicagel 60.

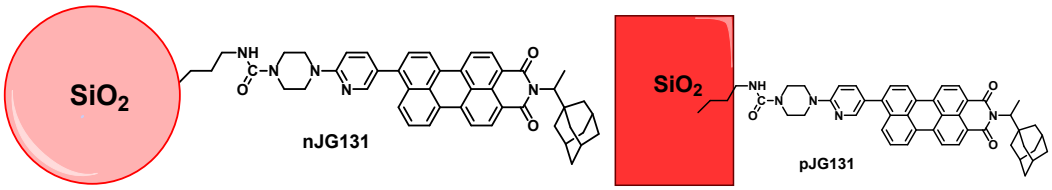

Figure S30. Silica derivatives of JG131, in silica nanoparticles (n) and in a TLC (p)

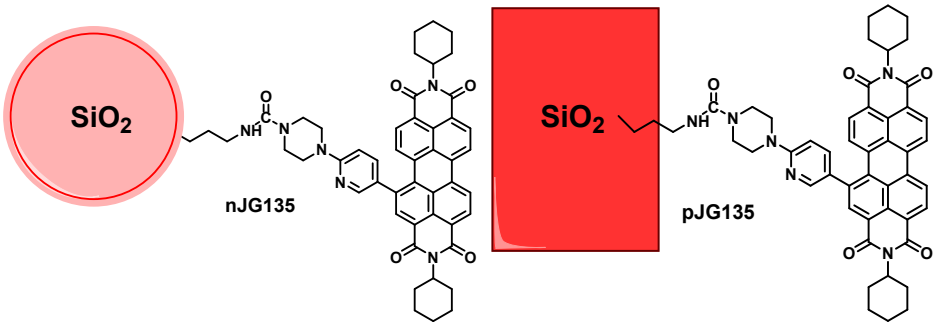

Fig S31. Silica derivatives of JG135, on silica nanoparticles (n) or on TLC plates (p)

Functionalized silica nanoparticles were prepared from 500 mg of silica nanoparticles and 4 mg of the triethoxysilyl perylene derivative. The mixture was refluxed at 112ºC in a mixture of Toluene:Water 500:10 µL for 24 hours. Finally, the nanoparticles were washed with 2 x toluene, 2 x DCM and 2 x Et_2O. The products obtained were called **nJG131** and **nJG135**.

By the same way the silane derivatives were bonded to silica TLC plates, 0.5 mg of JG131 or JG135 for every 5×10 cm plate. Instead of putting it under reflux, it was heated at 60ºC for 48 hours, until the solutions had neither color nor fluorescence. Then, the TLC plates were cleaned by the same procedure. The products obtained were called **pJG131** and **pJG135**.

In addition to this synthesis, JG125 and PC63 were put under the same process than to obtain pJG131 and pJG135. However, in this case it is an adsorption process, obtaining the product adsorbed in silica, these products were called **pJG125** and **pPC63**.

2.3. Characterization of the functional materials

The whole quantity of **nJG131**, **nJG135**, **pJG131**, **nJG135**, **pJG125** and **pPC63** reacted or adsorbed in the silica leaving colorless solutions. The silica nanoparticles were characterized by checking the fluorescent profiles, emission and excitation.

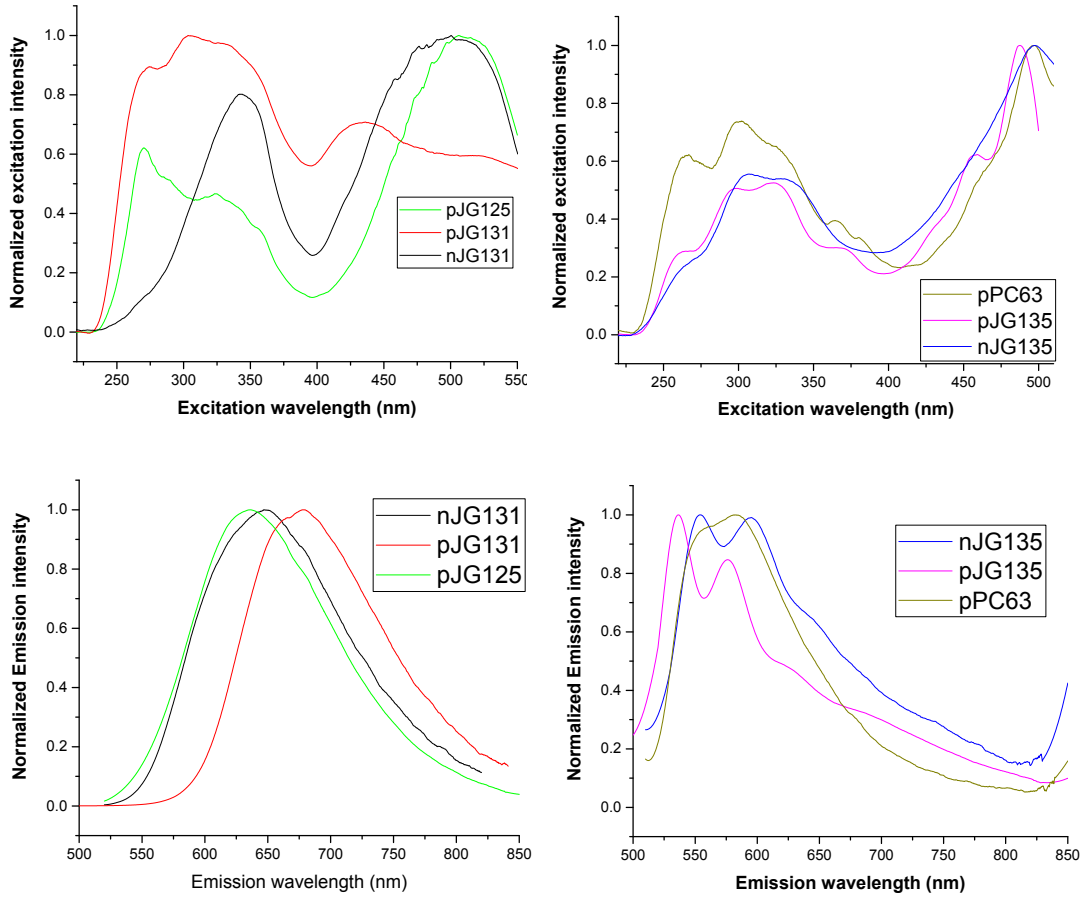

Figure S32: Normalized Emission (up) and excitation (down) spectra of the supported probes in silica.

The proportions of carbon/silicon were also checked by **EDX analysis** (Energy-dispersive X-ray spectroscopy).

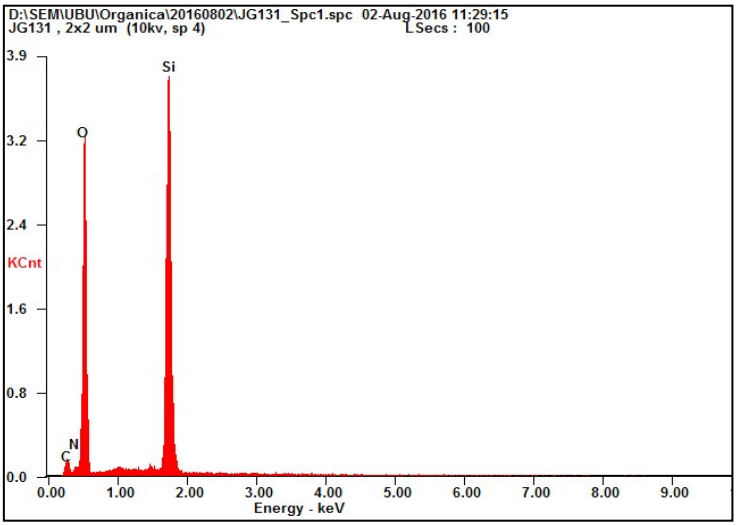

Figure S33. EDX profile of pJG131.

From the different profiles, the proportion Si/C obtained were around 2-5 % in case of the silica nanoparticles and 5-8 % for the TLC plates. These results are in agreement with the supposed proportions of carbon due to the quantity of perylene added, 2.8 % for the silica nanoparticles. For the TLC plates, the supposed proportion couldn't be calculated but the results are quite close.

In addition to this, TGA was performed for the nanosilica substituted materials **nJG131** and **nJG135**.

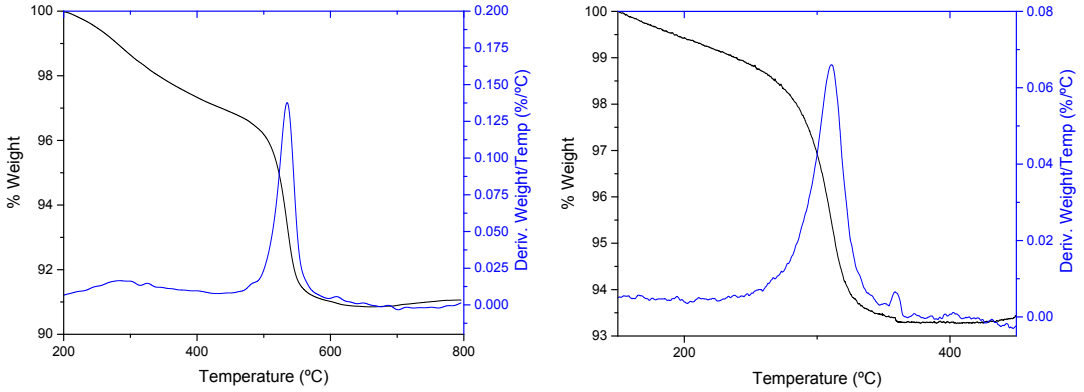

Figure S34. TGA in N_2 of nJG131 (left) and nJG135 (right).

nJG135 and **nJG131** lost 6-8 % weight, corresponding to the presence of organic matter, presumably perylene derivative in each case.

Furthermore, a peak of weight loss was observed in the silica substituted with perylene monoimide at 300 ºC temperature, which is in agreement with the degradation when calculating the melting point.

3. SOLVATOCHROMISM:

The probes **JG125** and **PC63** (Boc-protected probes) and **JG125d** and **PC63d** (deprotected) have properties as potential oxidant detectors, which was detected in preliminar testing. Then, the general behavior was studied in solution.

The solvatochromism of compounds **JG125** and **PC63** (10 µM) is useful for studying the effect and the solubility of the probes in different solvents, because of that, it is the first step in the study of these compounds, the studied solvents were:

1. Water
2. MeOH
3. DMSO
4. DMF
5. MeCN
6. Acetone
7. AcOEt
8. THF
9. $CHCl_3$
10. CH_2Cl_2
11. Toluene
12. Et_2O
13. Hexane
14. Cyclohexane

JG125:

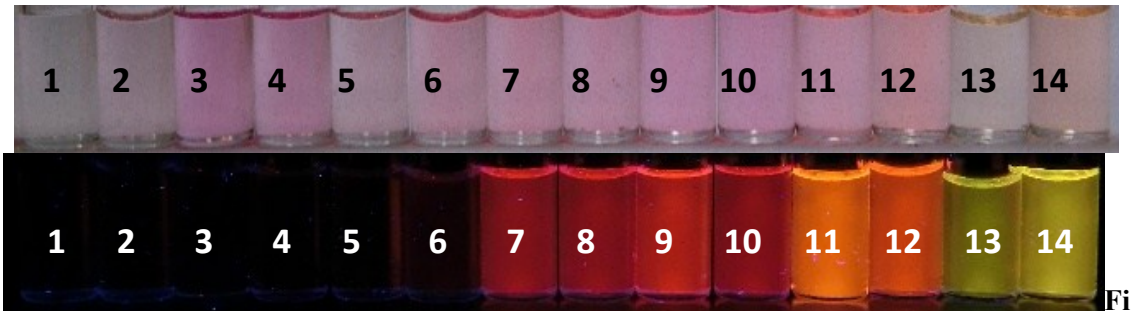

Figure S35. Solvatochromism JG125, under visible light (up) and under UV light (down).

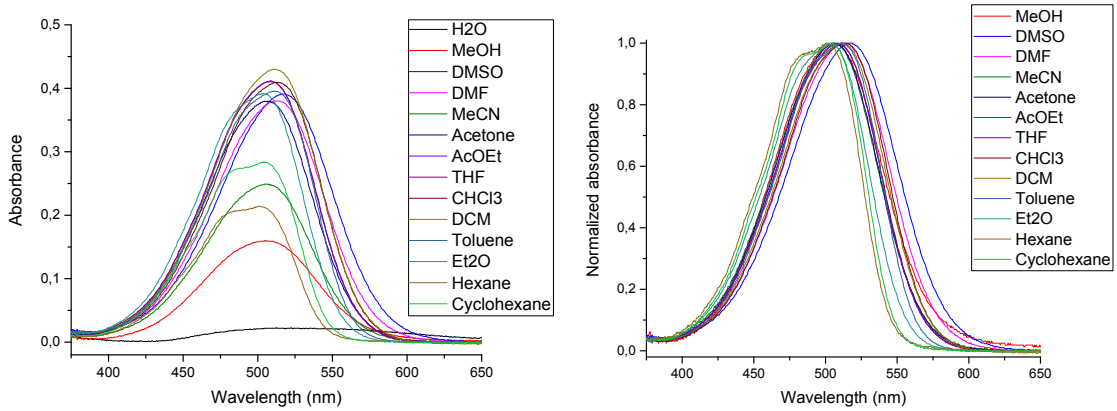

Figure S36. Solvatochromism JG125, absorbance in different solvents.

The change in the wavelength of absorbance is batochromic with the polarity but not very significant, the solubility is very low in water, methanol, hexane, acetonitrile and cyclohexane and when the polarity is very low a shoulder at lower wavelengths may be seen, probably a band that is less overlapped with less polarity.

The fluorescence was measured by excitation with light at 512 nm:

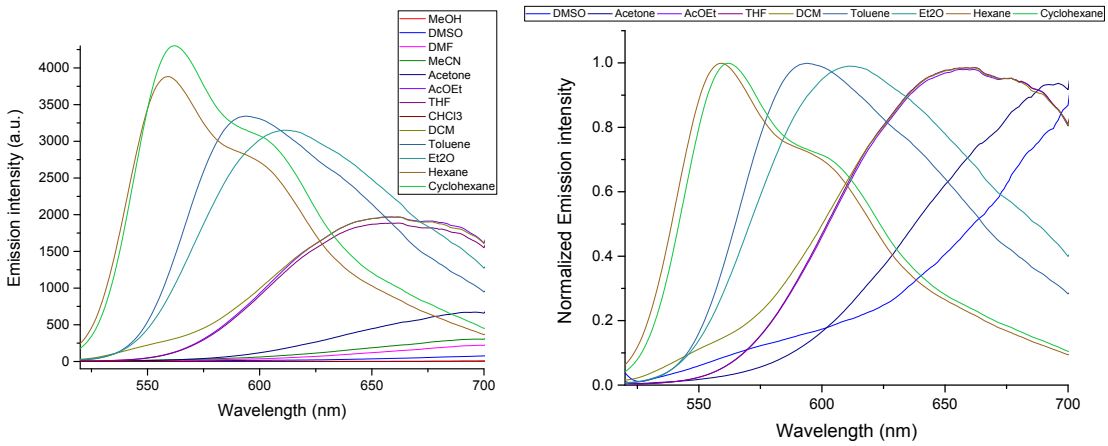

Figure S37. Solvatochromism JG125, fluorescence response when λ_{exc} = 512 nm, in different solvents.

The conclusions are similar to absorbance, but the batochromic effect is much more intense, having the maximum of intensity at $\lambda \geq 700$ nm and the intensity of emission is higher when the polarity of the solvent is lower.

JG125d:

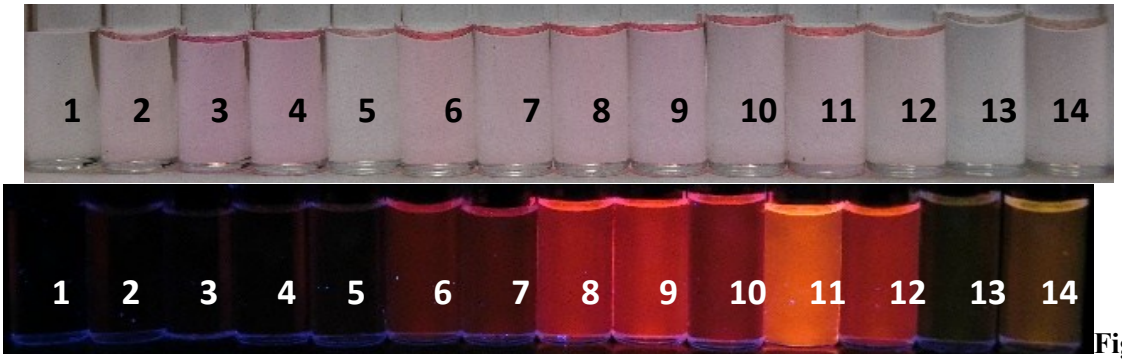

Figure S38. Solvatochromism JG125-deprotected, under visible light (up) and under UV light (down).

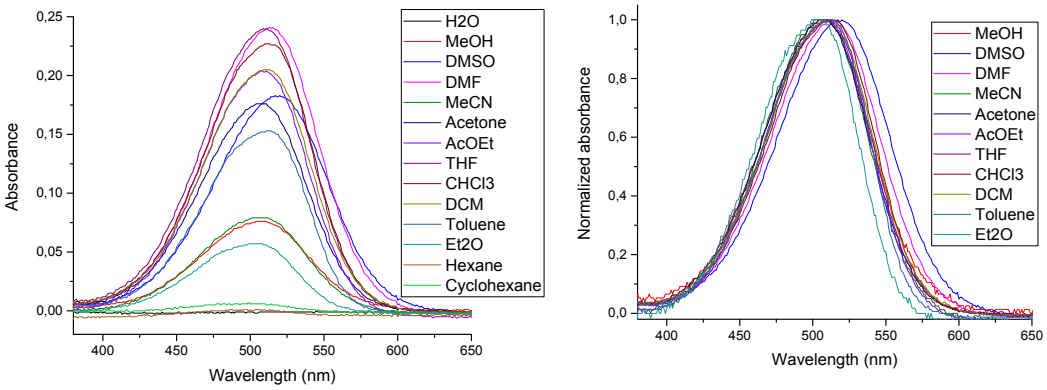

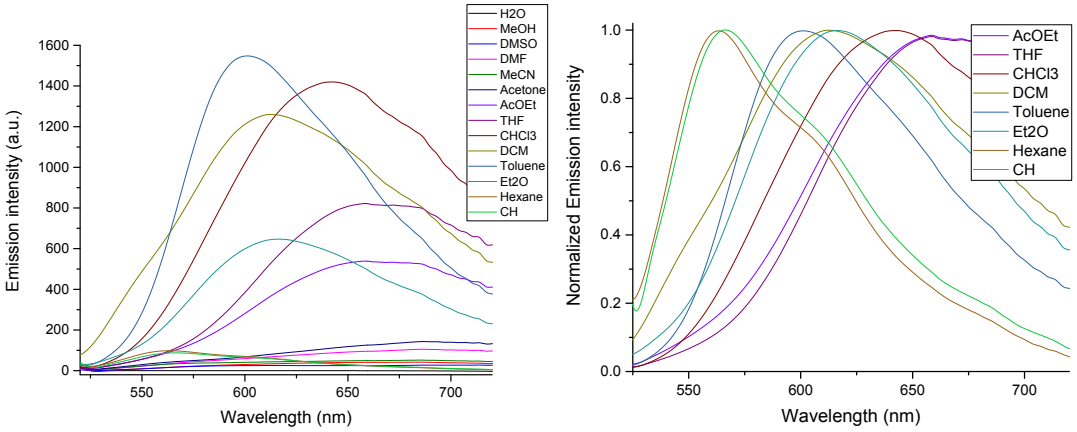

Figure S39. Solvatochromism JG125d, absorbance in different solvents (up) and fluorescence response when λ_{exc} = 512 nm (down).

JG125d has very similar behavior of **JG125**, but the color and fluorescence are less intense.

The greatest absorbance was measured in Et_2O, THF, DMF and DCM.

- Et_2O is too volatile.
- Solvents more polar than AcOEt show a maximum of emission beyond 700 nm.
- DMSO and DMF are hard to evaporate and the fluorescence is negligible.
- THF could lead to secondary reactions with peroxides.
- CH_2Cl_2 shows good solubility, but is too volatile.

PC63:

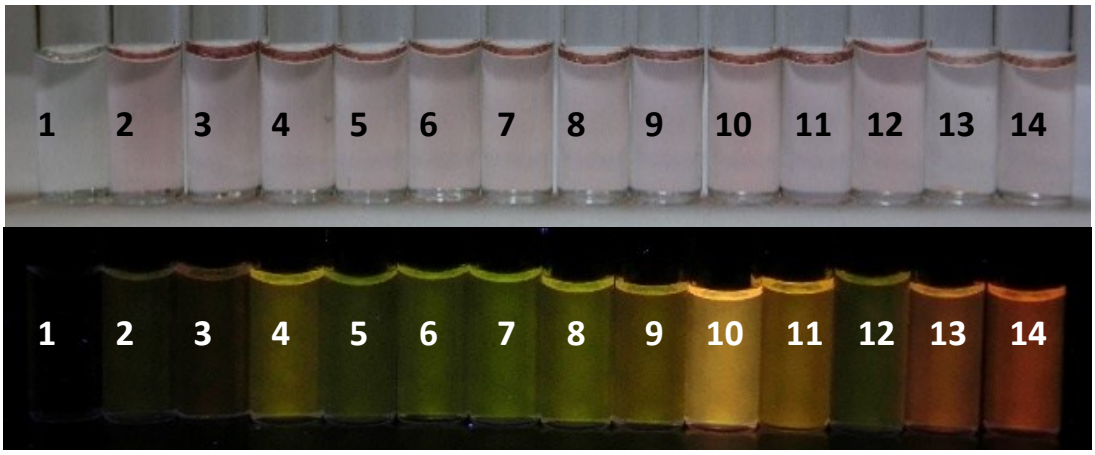

Figure S40. Solvatochromism PC63, under visible light (up) and under UV light (down).

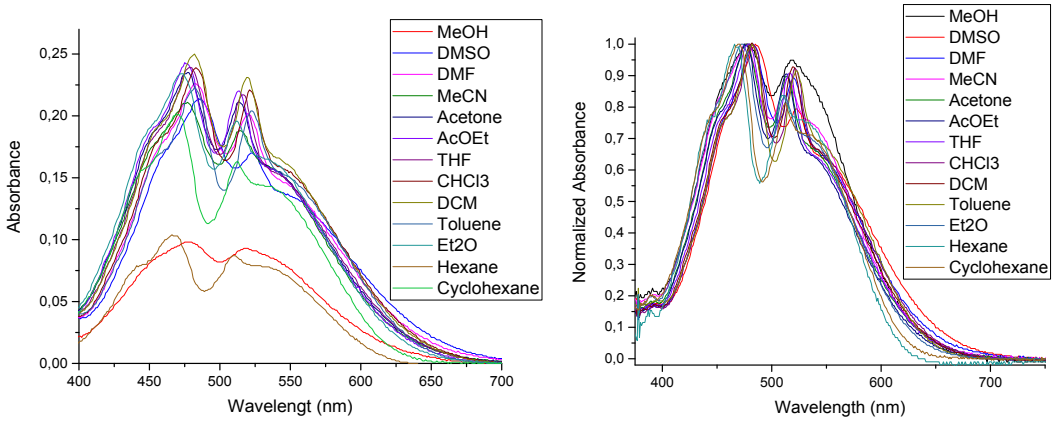

Figure S41. Solvatochromism PC63, absorbance in different solvents.

The change of the maximum absorption is very low between solvents, however a decrease in polarity makes the band get more stretched and the presence of several overlapped bands may be clearly distinguished.

The fluorescence was measured by excitation at 483 nm:

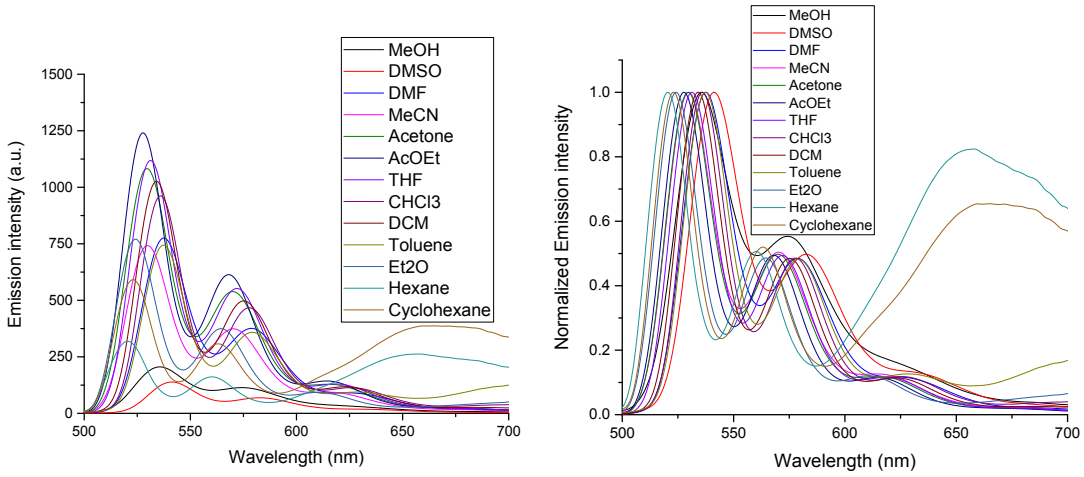

Figure S42. Solvatochromism PC63, fluorescence response when λ_{exc} = 483 nm, in different solvents.

The change in absorbance is hypsochromic with an increase in polarity the opposite than JG125, furthermore, the overlapping of the bands with polarity can be clearly observed too. An increase in the emission at 650-700 nm can also be observed in hexane and cyclohexane

PC63d:

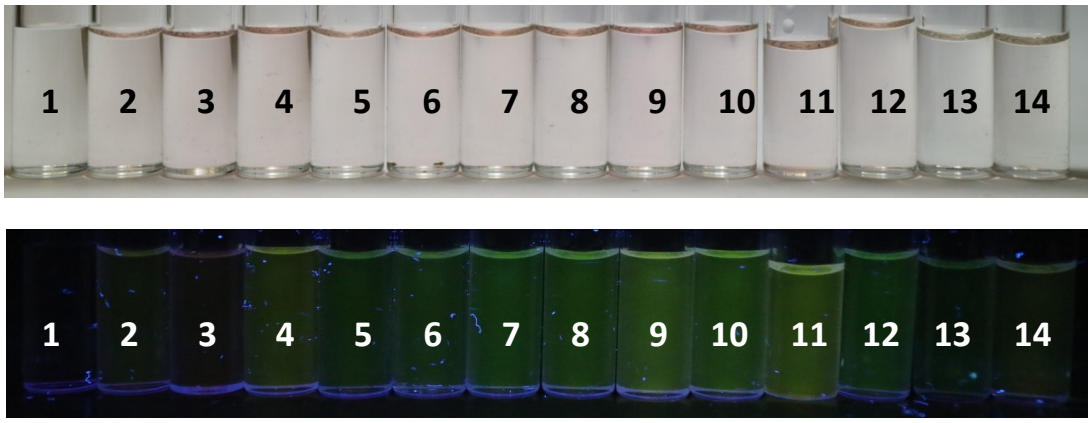

Figure S43. Solvatochromism PC63d, under visible light (up) and under UV light (down).

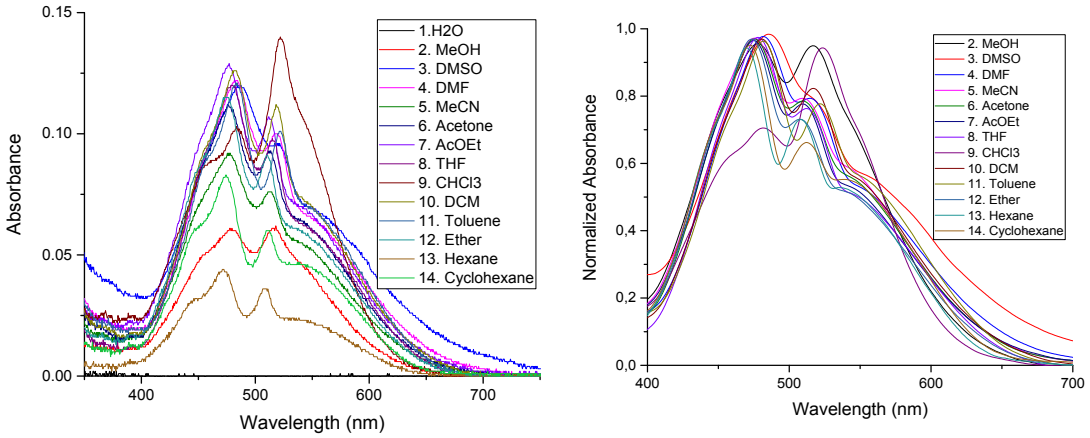

Figure S44. Solvatochromism PC63d, absorbance in different solvents.

The fluorescence was measured by excitation with light at 483 nm:

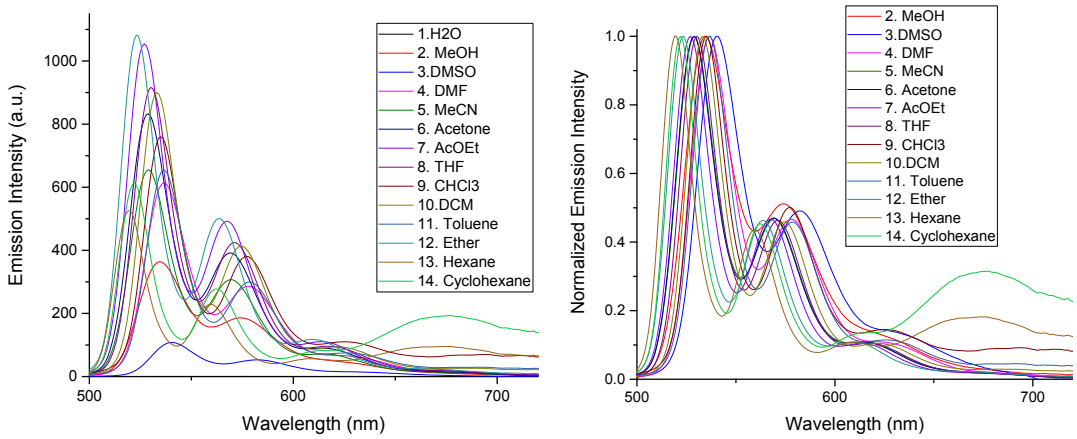

Figure S45. Solvatochromism PC63d, fluorescence response when λ_{exc} = 483 nm, in different solvents.

The response to the solvents was very similar to **PC63** but less remarkable and more similar between them. In consequence, **the chosen solvent was $CHCl_3$**, less volatile than CH_2Cl_2. In order to dissolve the peroxides it is necessary to add a secondary solvent in which it is possible. It was checked that 10% of methanol was enough.

4. Qualitative and quantitative measures of JG125 and PC63:

4.1. Qualitative response of solutions to different oxidants:

The fluorescence of the probes increases in presence of oxidant species, but only in the case of Boc protected probes and not in the deprotected ones. This process is also useful in order to make materials that are sensitive to oxidants, previously deprotected and bound to the material covalently, by formation of a new amide group.

Before the quantitative measurements, the probes were tested with several oxidative reagents. All the probes were dissolved in $CHCl_3$:MeOH 9:1. The reason for using solvent mixtures is because of the minimal change respect $CHCl_3$ solutions and the increase of solubility of oxidants insoluble in organic media. The change under visible and UV light was registered.

500 µL solutions of JG125 and PC63 are prepared in $CHCl_3$:MeOH 9:1, then, 10 µL of the next solutions were added:

A) Nothing
B) HEPES 0.5 M in water.
C) HCl 0.01M in water.
D) TATP 0.2 M in $CHCl_3$.
E) MCPBA 0.2 M in $CHCl_3$.
F) Oxone 0.2 M in water.
G) TNB 1mg.

JG125

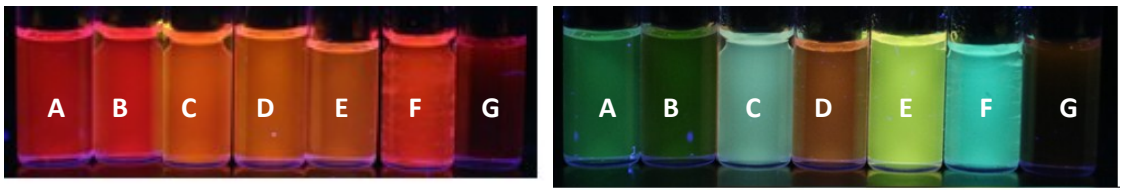

Figure S44. Response under UV light of JG125 (left) and PC63 (right) against different oxidant species.

From this study, apparently, JG125 is more sensitive to oxidants like TATP and mCPBA. In contrast, the change in the emission is more significant with PC63, from green to orange. These results were corroborated by the quantitative analysis afterwards.

4.2. Work concentration:

In order to choose an optimum concentration for the quantitative studio, the absorbance and fluorescence of the probes was checked to be linear while concentration changes are small. Studied $CHCl_3$:MeOH 9:1, **JG125** is showed as an example:

JG125

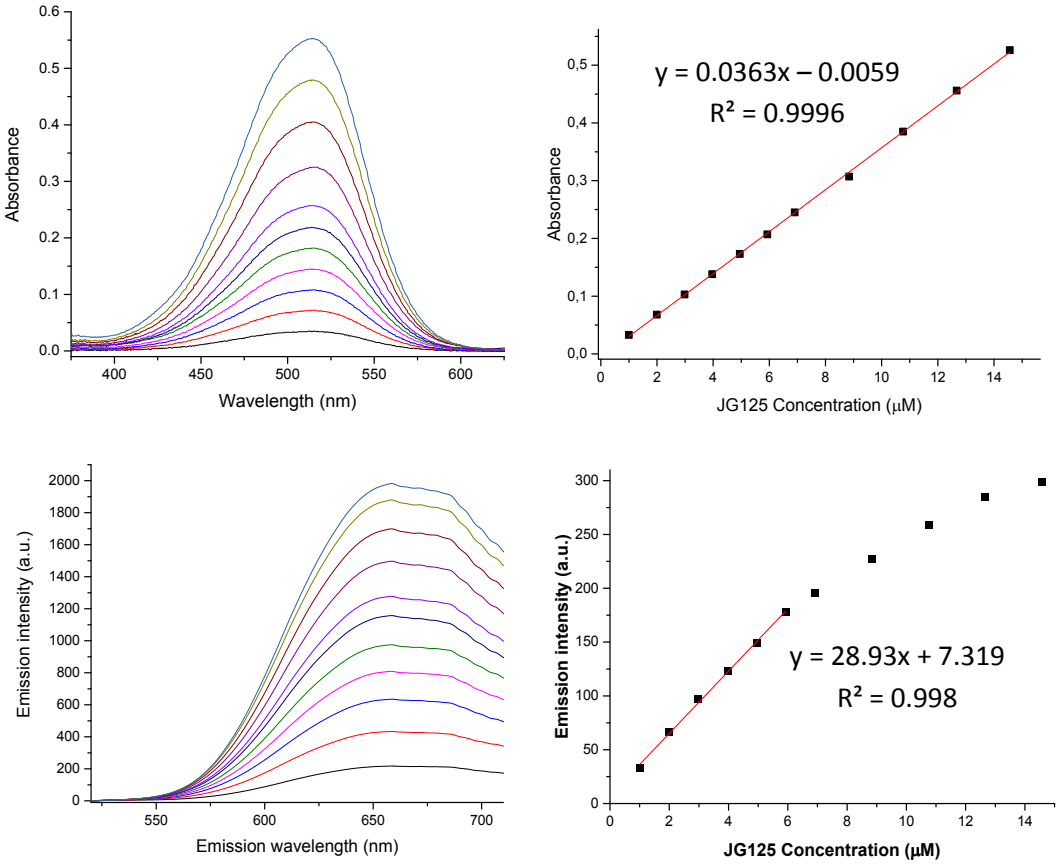

Figure S47. Absorbance (up) and fluorescence (down) of JG125 solution in $CHCl_3$:MeOH 9:1, under increasing concentrations of JG125, λ_{exc} = 512 nm (down).

JG125 + MCPBA excess:

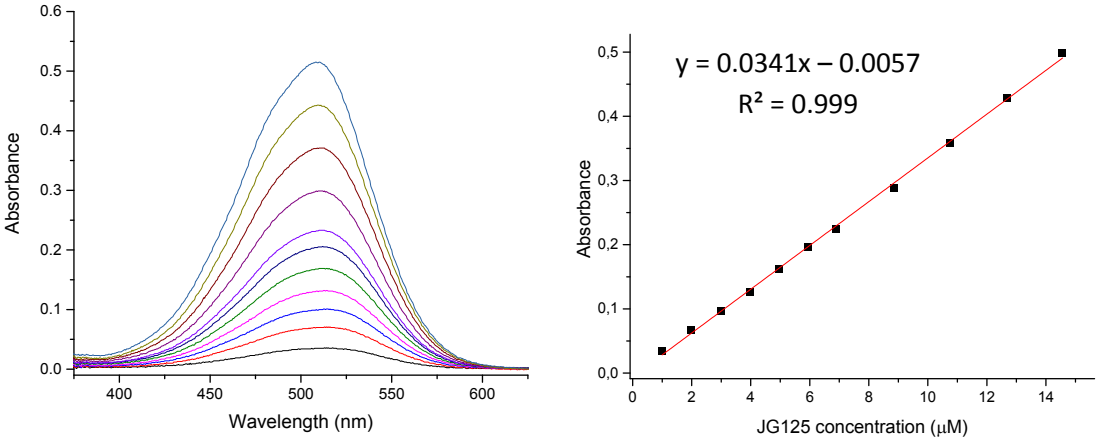

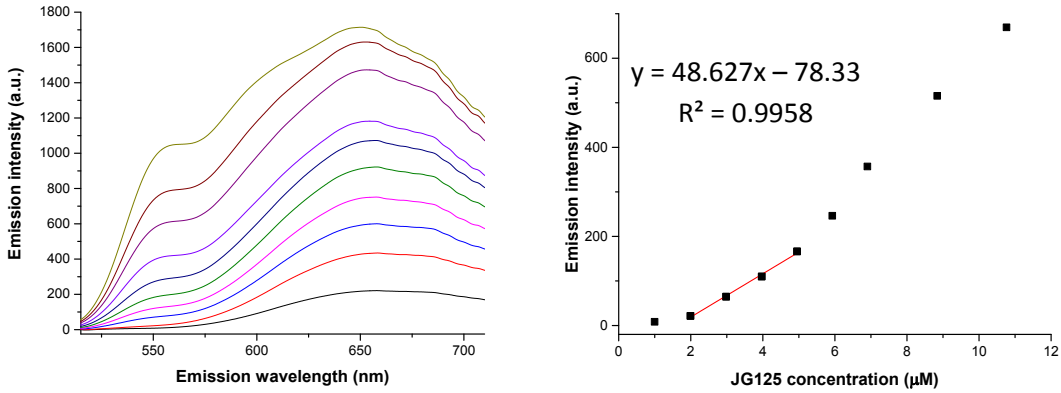

Figure S48. Absorbance (up) and fluorescence (down) of JG125 solution in $CHCl_3$:MeOH 9:1, under increasing concentrations of JG125 and excess MCPBA.

The maximum the fluorescence increases at 560 nm after adding the oxidant. The work concentration ideally should be at 0.1 of absorbance or less, to avoid inner filter effects and possible dynamic quenching or stacking processes. Therefore, the chosen concentration was 2.5 μM, value around which the Lambert-Beer law is fulfilled.

4.3. Quantitative measures of probes vs TATP and mCPBA in solution:

In order to determine the behavior of **PC63 and JG125** with oxidants, the measurements carried out were the next ones:

I. TATP titration: optical changes and the limit of detection.

II. MCPBA titration: optical changes and the limit of detection.

The limit of detection was also calculated for both probes. The emission was adjusted to a minimum squares linear regression. The sloped is checked to be different of zero and without presence of outliers.
Then, with the program "R", the limit of detection associated to the linear regression was calculated. In order to obtain a reliable limit, the values of false positive and false negative were fixed as equal or inferior to 5%.

I. Titration of JG125:
A solution of JG125 (2.5·μM) in $CHCl_3$:MeOH 9:1 were prepared.
The conditions were:

- The concentration of TATP and mCPBA was increased by adding from a concentrated solution in the same solvent.
- λexc = 500 nm, λem = 556 nm.
- The absorbance and fluorescence changes were registered at 25 ºC.

TATP titration:

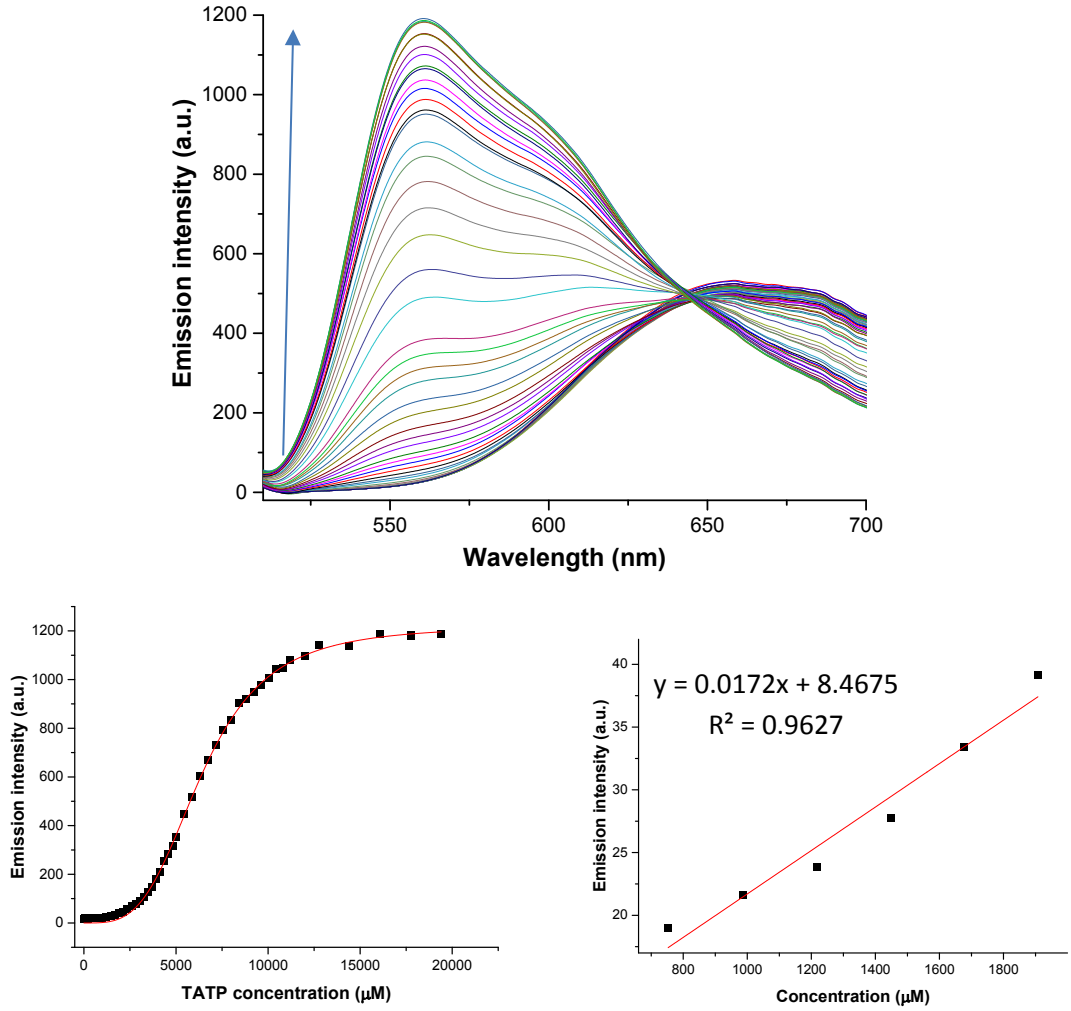

Figure S49. Titration (up), fluorescence profile at 556 nm (down-left) and calibration for the limit of detection (down-right) of JG125 solution 2.5 μM in $CHCl_3$:MeOH 9:1, under increasing concentrations of TATP.

The limit of detection was **620 μM or 0.27 mg** in a 2.5 ml solution.

mCPBA titration:

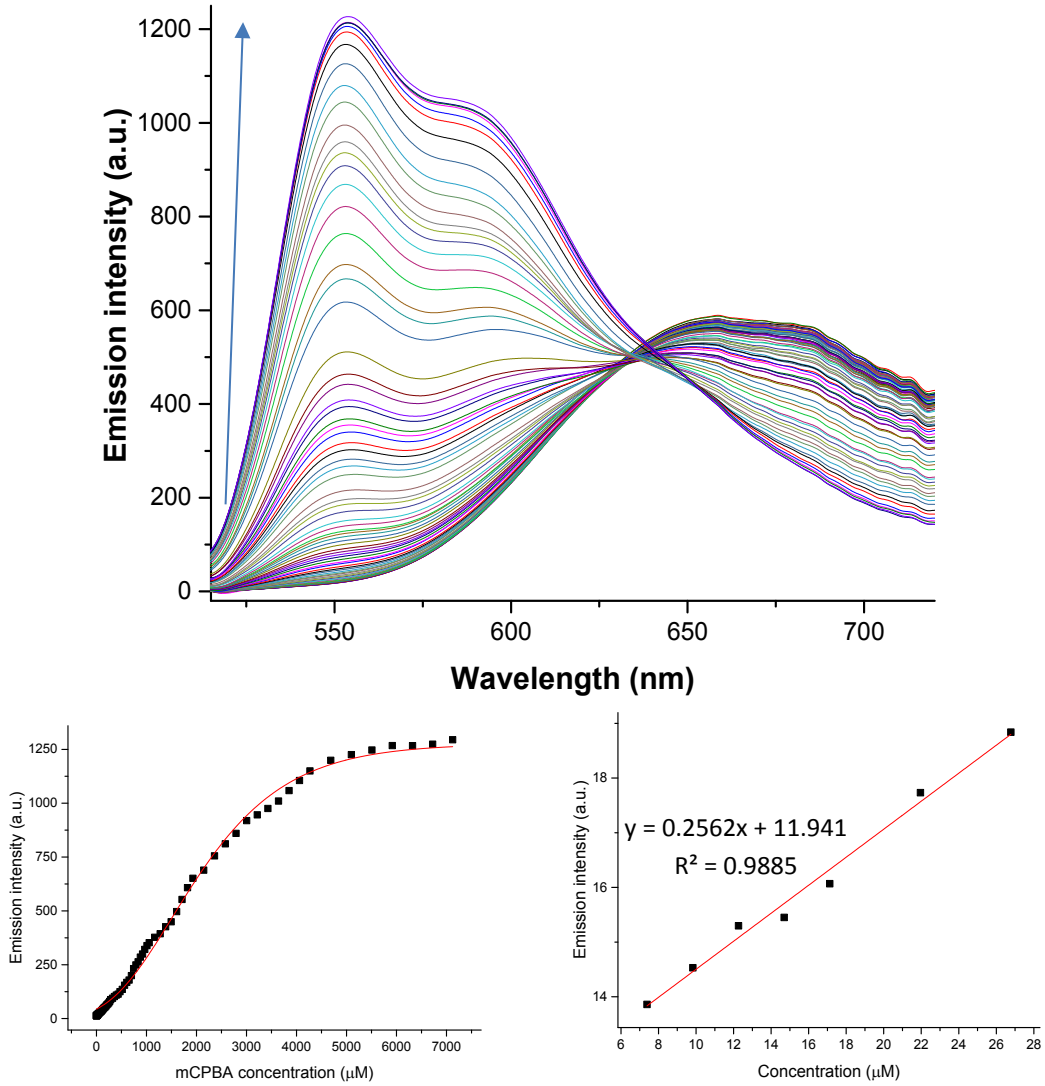

Figure S50. Titration (up), fluorescence profile at 556 nm (down-left) and calibration for the limit of detection (down-right) of JG125 solution 2.5 μM in $CHCl_3$:MeOH 9:1, under increasing concentrations of mCPBA.

The limit of detection was **7.4 μM or 0.0032 mg** in a 2.5 ml solution.

II. Titration of PC63:

A **PC63** solution (2.5 μM) in $CHCl_3$:MeOH 9:1 was prepared.
The conditions were:

- The concentration of TATP and mCPBA was increased by adding aliquots from a concentrated solution in the same solvent.
- λexc = 484 nm, λem = 536 nm.
- The absorbance and fluorescence changes were registered at 25 ºC.

TATP titration:

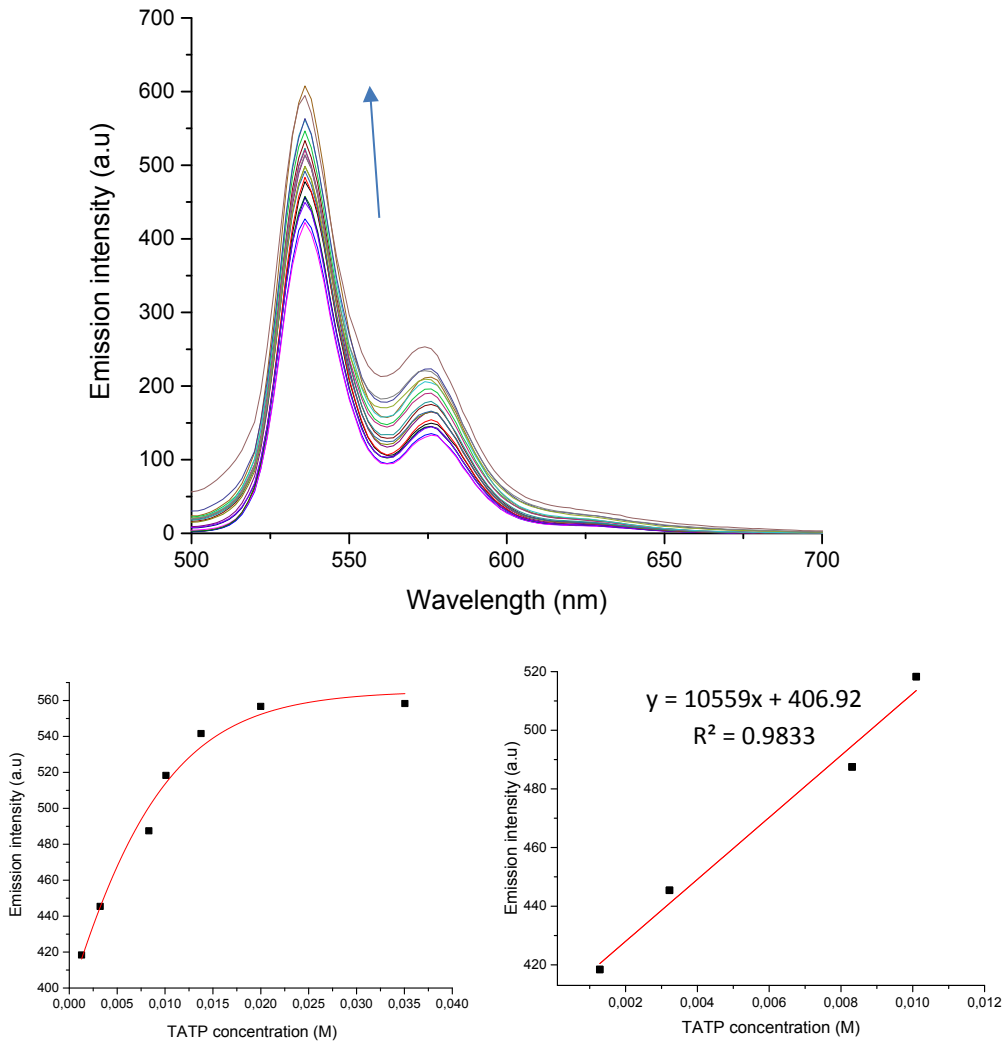

Figure S51. Titration (up), fluorescence profile at 536 nm (down-left) and calibration for the limit of detection (down-right) of PC63 solution 2.5 µM in $CHCl_3$:MeOH 9:1, under increasing concentrations of TATP.

The limit of detection was **4.83 mM or 2.1 mg** in a 2.5 ml solution.

mCPBA titration:

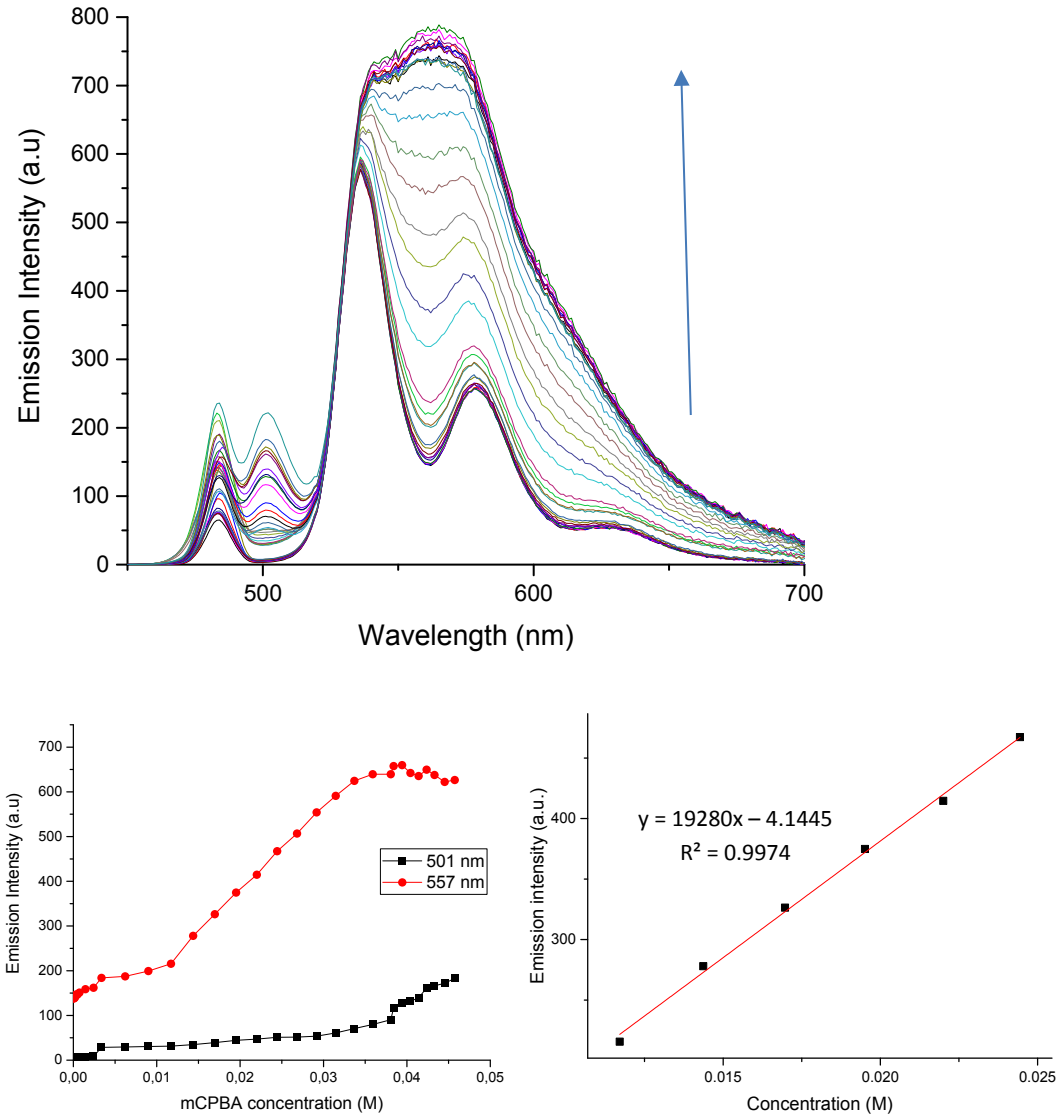

Figure S52. Titration (up), fluorescence profile at 536 nm (down-left) and calibration for the limit of detection (down-right) of PC63 solution 2.5 µM in $CHCl_3$:MeOH 9:1, under increasing concentrations of MCPBA.

The limit of detection was **3.2 mM or 1.4 mg** in a 2.5 ml solution.

There are two fluorescent responses for the increase of MCPBA concentration, between 3 mM to 32 mM the increase is at 557 nm, then, the fluorescence increases at 501 nm, appearing a new band.

4.4. Quantum yield and lifetime measurements

Quantum yield was determined by its general equation:

$$\Phi = \Phi_R \frac{n^2 A_R F}{n_R^2 A F_R}$$

Where

- Φ is the quantum yield.
- n represents the refractive index of the solvent.
  - n(EtOH) = 1.362
  - n($CHCl_3$) = 1.458
- A is the absorbance.
- F is the fluorescence.
- R means that the parameter is associated to a reference sample.

Parameters:

- The chosen reference was Rhodamine 6G.
- The integral was done between 480 – 800 nm, and the Rayleigh signal was deconvoluted.

The process was repeated three times to obtain the media and a confidence interval. Keeping in mind that the error associated to the method is 1 %, higher than the experimental results.

So:

Φ_{JG125} ($CHCl_3$) = 0.23 ± 0.01
$\Phi_{JG125+TATP}$ ($CHCl_3$) = 0.65 ± 0.01
Φ/Φ_0 = 2.8
Φ_{PC63} ($CHCl_3$) = 0.27 ± 0.01
$\Phi_{PC63+TATP}$ ($CHCl_3$) = 0.36 ± 0.01
Φ/Φ_0 = 1.33

5. TATP DETECTION IN MODIFIED SILICA:

Several samples were tested as potential TATP sensors, it can be distinguished 3 kinds of modified silica and two probes, the monoimide derivatives (**JG125**) and diimide derivatives (**PC63**):

- Modified silica nanoparticles (**nJG131** and **nJG135**): 4 mg of probe every 500 mg of silica.
- Modified supported silica (**pJG131** and **pJG135**): 0.5 mg every 5×10 cm layer.
- Silica adsorbed probes (**pJG125** and **pPC63**) were studied: 0.5 mg every 5x10 cm layer.

The ratio probe/silica can be altered obtaining different results. The change is the intensity of the color and, specially, in fluorescence. Therefore, it was chosen the optimum ratio to show a clear increase in fluorescence.

The changes in fluorescence were compared between different vapors:

Nothing – TATP – HCl – H_2O_2

The HCl samples increase the fluorescence in all cases, however, this process is different from the increase with TATP. After being under vapors of an amine, like Et_3N, the fluorescence of the HCl samples decreases again, a process that does not occur for TATP.

So as to measure the increase in fluorescence with TATP, the flux of N_2 was controlled to be 100 cm^3/min and the temperature in the TATP flask around 55 ºC, going through a flask with 2 mg of TATP. Being able to detect changes in the fluorescence of the probes within several minutes.

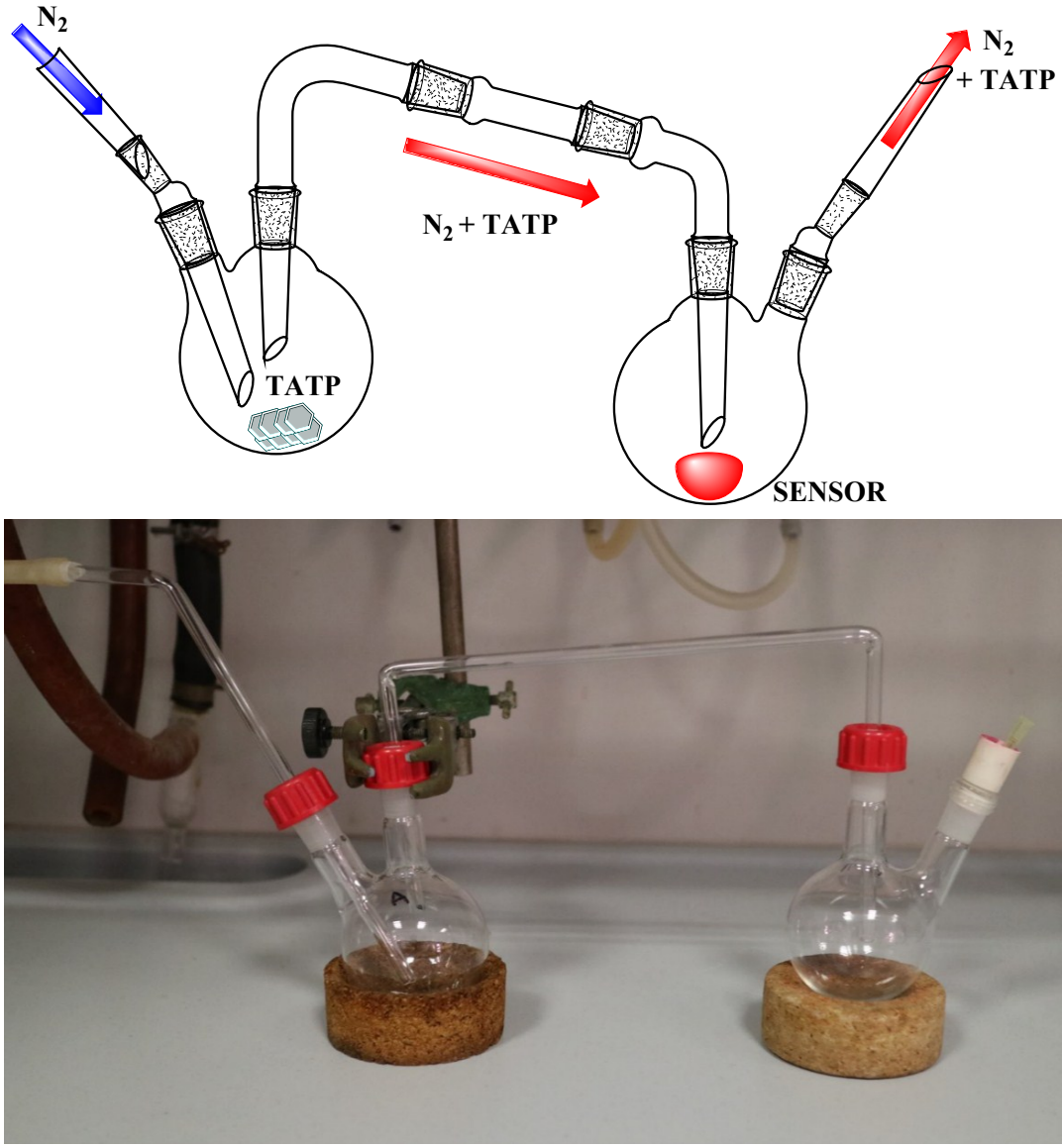

Figure S53. System to measure a TATP current with the supported sensor.

The changes were studied by several methods that gave different information about the sample:

- As a **code of colors from the pictures of fluorescent changes**. It may be compared in order to detect qualitatively the presence of TATP in the environment, comparing with the initial color. It has to be taken into account that the absorbance and fluorescence depend on the amount of the probe that there is on the silica. (showed in the paper)
- Then, the **increase in fluorescence** in solids was measured by calculation of the quantum yield and measuring the increase directly in the solid. The quantum yield depends on the quantity of the probe that is contained, providing that the quantity of probe is not too high or too low. It would be possible to measure changes in fluorescence by only fluorescence intensity, however, the measures are sometimes dependent on the position of the solid in the sample and factors difficult to control without designing a device for doing so. As a consequence, quantum yields are the most trustworthy way to measure it quantitatively.
- The spectra were normalized in order to obtain information from the **position of the excitation and emission peaks**, which is a way to distinguish between oxidants.

5.1. Quantitative study of the presence of the peaks, excitation and emission in fluorescence:

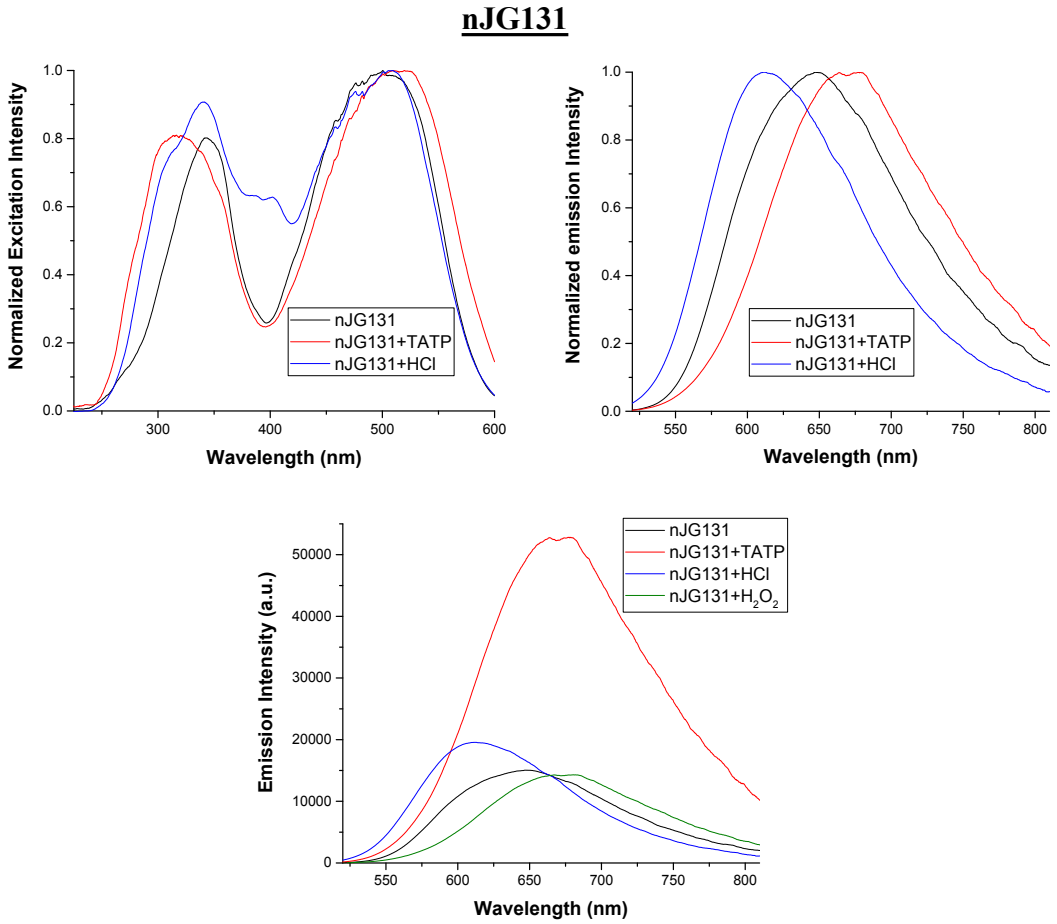

Figure S54. Response in excitation and fluorescence of nJG131. λexc = 492 nm, λem = 614 nm.

pJG131

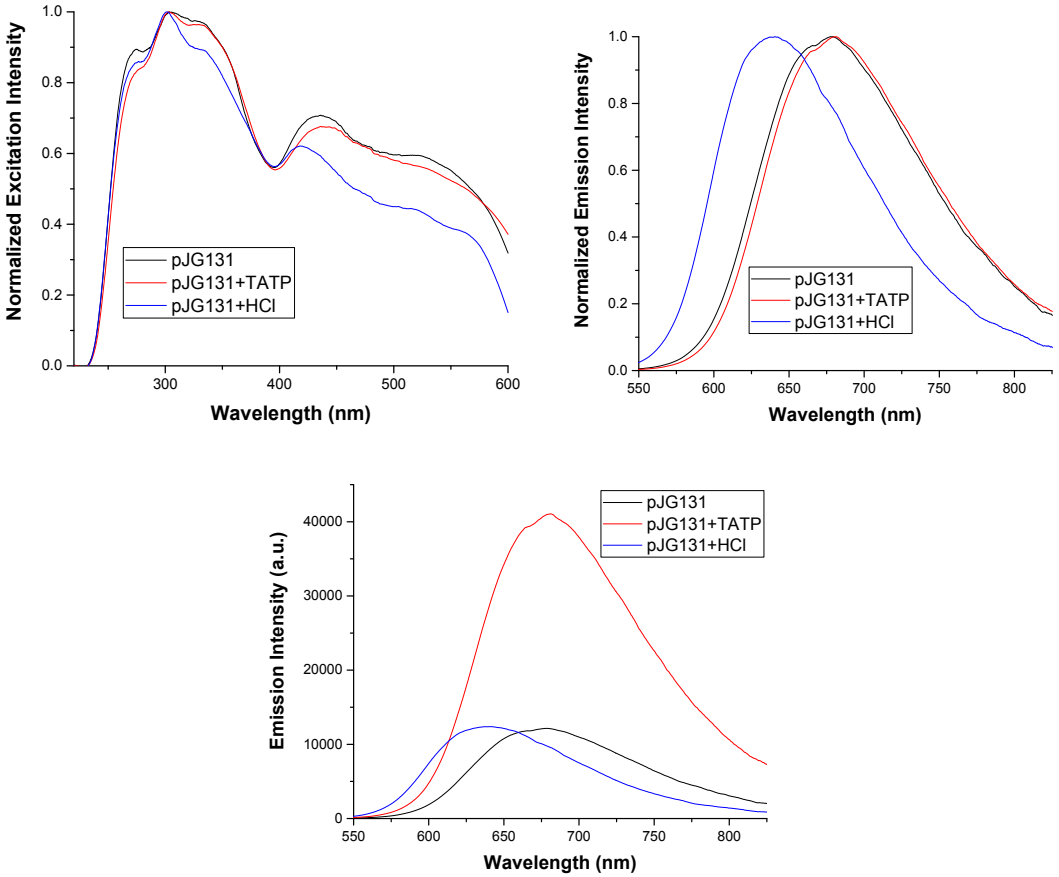

Figure S55. Response in excitation and fluorescence of pJG131. λexc = 438 nm, λem = 630 nm.

aJG125 adsorbed on TLC plates

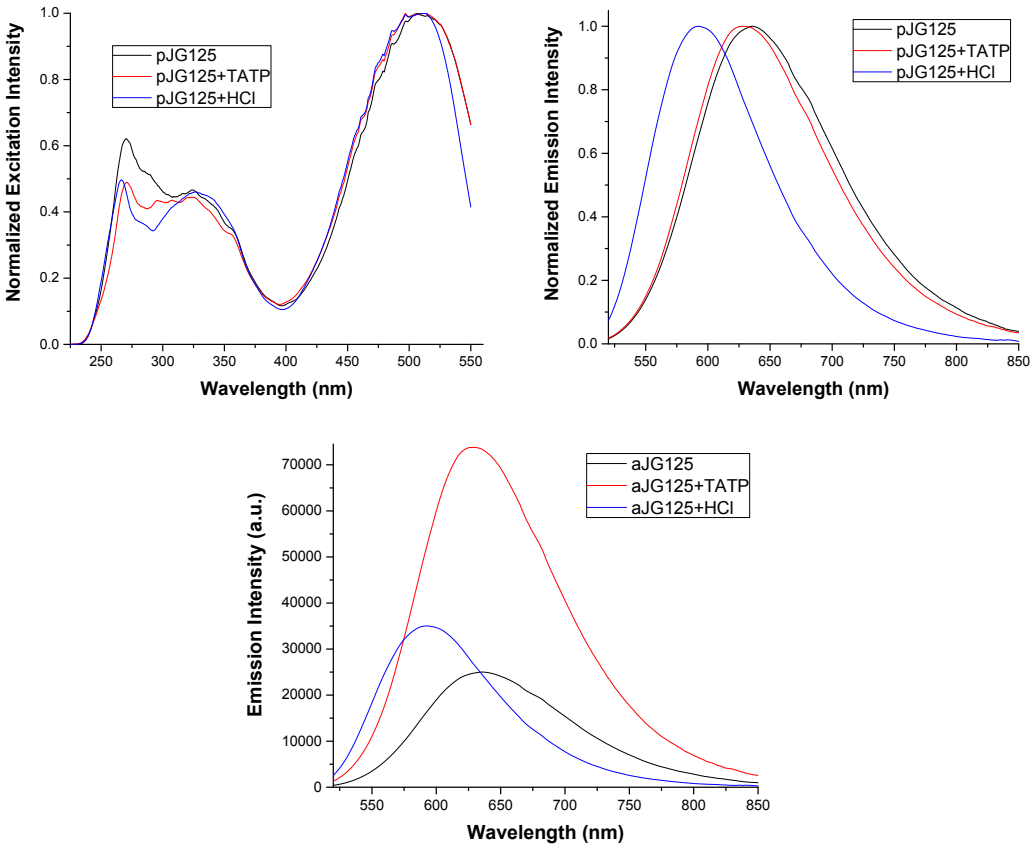

Figure S56. Response in excitation and fluorescence of abs aJG125. λexc = 500 nm, λem = 605 nm

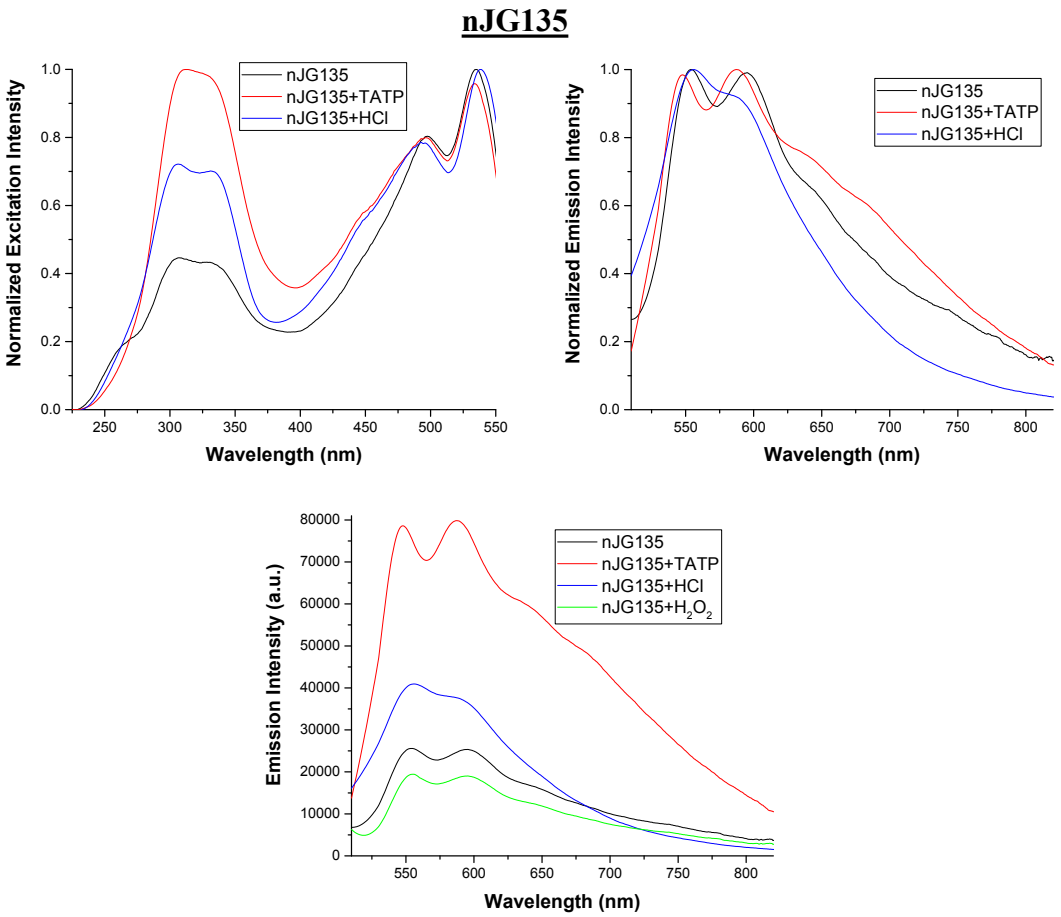

Figure S57. Response in excitation and fluorescence of nJG135. λexc = 495 nm, λem = 592 nm

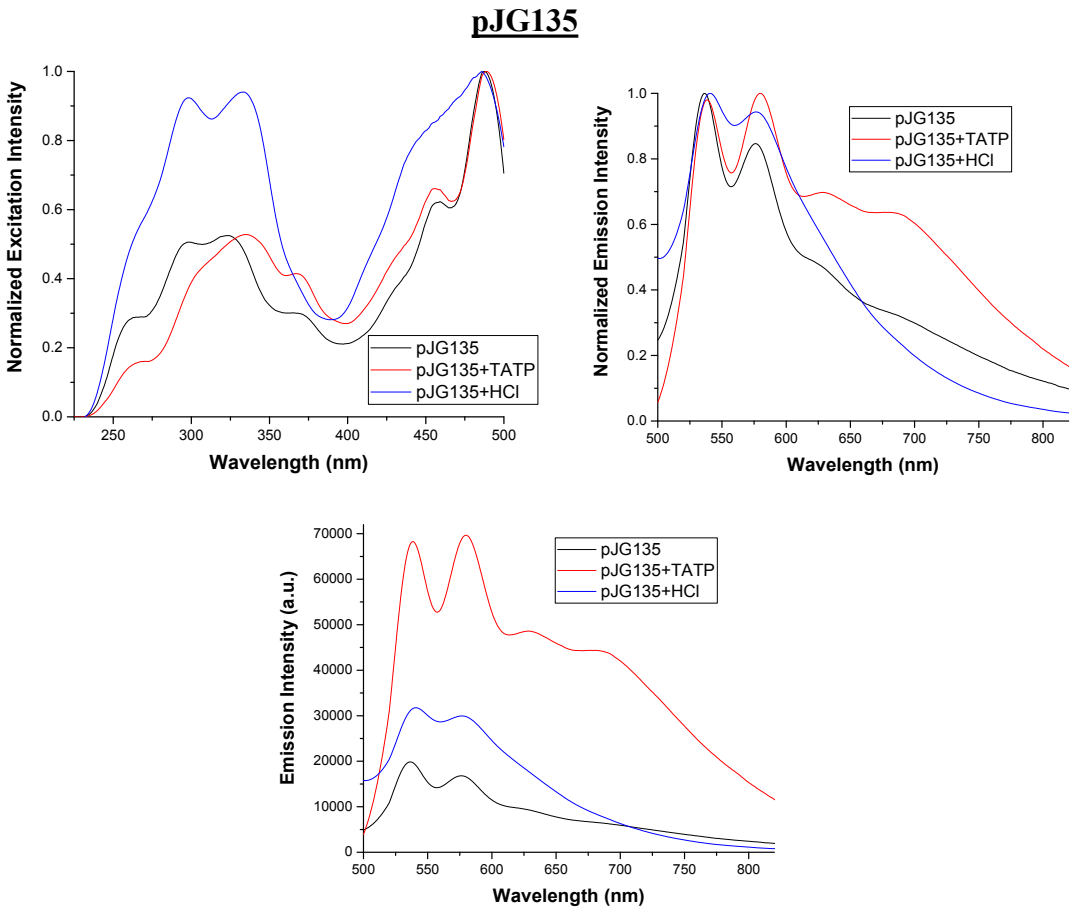

Figure S58. Response in excitation and fluorescence of pJG135. λexc = 487 nm, λem = 533 nm

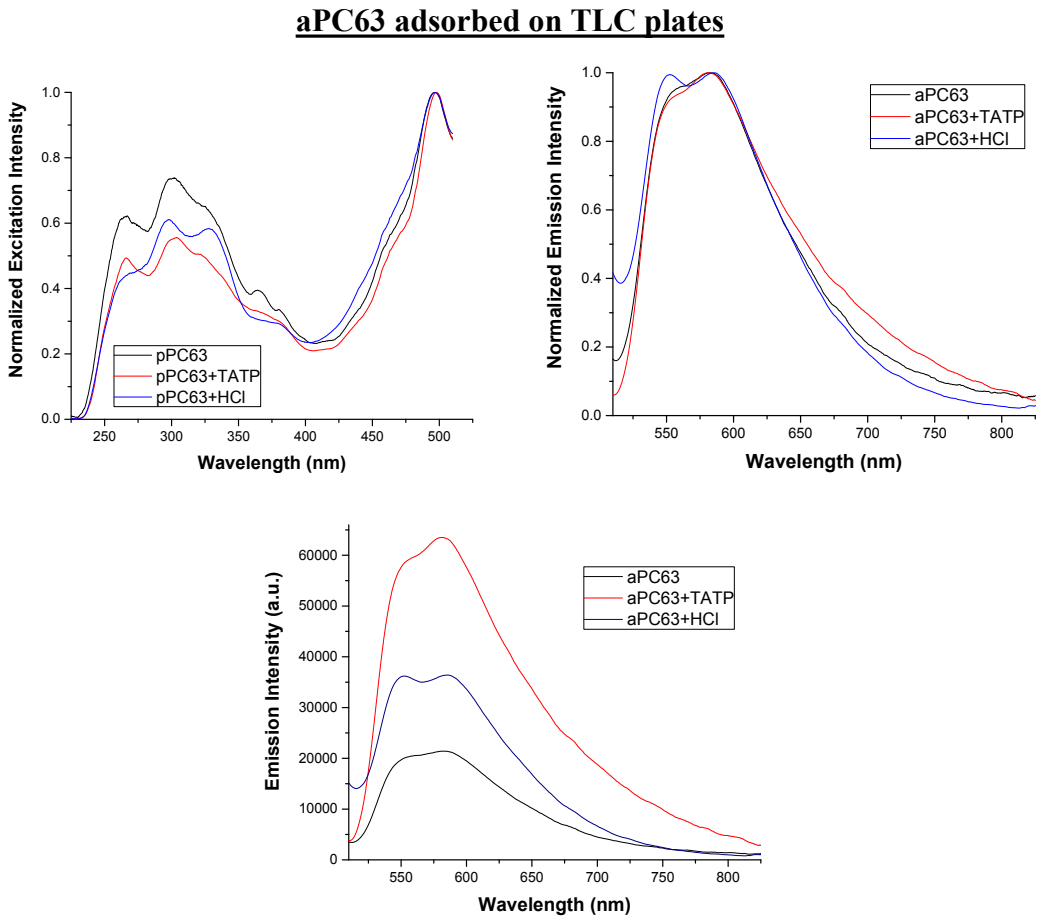

Figure S59. Response in excitation and fluorescence of pPC63. λexc = 496 nm, λem = 550 nm

These spectra allow us to distinguish between acid and TATP in several ways:

- The monoimide derivatives (**nJG131**, **pJG131** and **pJG125**) have a maximum of emission shift to lower wavelengths in presence of acids.
- The diimides (**nJG135**, **pJG135** and **aPC63**) increase their fluorescence at higher wavelengths only in presence of TATP
- In **nJG135** and **pJG135** the excitation at lower wavelengths, around 320 nm, changes depending on if it is TATP or HCl.
- **pPC63** does not show significant changes in the position of the bands.

5.3. Study of increment on the emission:

The most trustworthy method to measure with precision the increase in fluorescence of a material is by calculation of its quantum yield. To do so, it is necessary to have a fluorometer provided with an integration sphere, in this case a fluorometer Edinburgh Instruments FLS980. The precision of this method is checked by repeating three times each sample, it allows to obtain errors of less than 2%.

	Φ_{TATP}/Φ_0	Φ_{HCl}/Φ_0
nJG131	3.5	1.6
pJG131	3.4	1.0
aJG125	3.0	1.4
nJG135	3.1	1.6
pJG135	3.5	1.6
aPC63	3.2	1.7

Figure S60. Increase in fluorescence between the initial and after being under excess of TATP.

In all cases, the increase in fluorescence goes from 2-4 % to 7-15 %. It depends on the relation probe/silica.

As a general rule, the increase in fluorescence with the probes is situated between 3 to 3.5 times in all samples for TATP and less than 1.7 times with HCl samples.

5.4. Titration under increasing concentration of TATP

Previous testing conditions were performed under a flux of TATP and retired within a few minutes. So as to improve the precision, the increase in fluorescence was tested by measuring TATP quantum yield. The system would need to be coupled to a fluorometer in order to assure the exact quantity (continuous measurements).

Then, this experiment was performed to calculate the minimum amount in gas that produces a detectable response, the calibration was measured in steady state. Fixed quantities of TATP where vaporized in the presence of a sample containing 15 mg of silica nanoparticles and the fluorescence increase was measured.

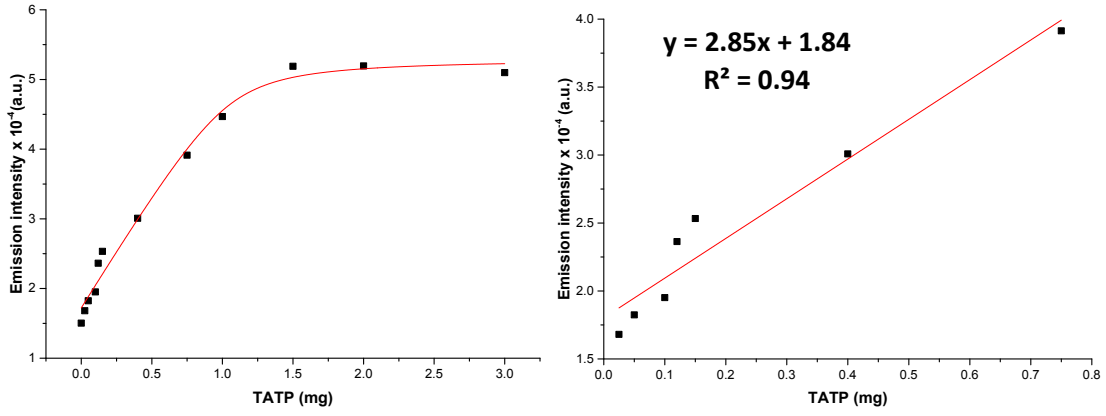

Figure S61. Calibration, adding increasing concentrations of TATP. of nJG131. λexc = 495 nm, λem = 620 nm.

By making a linear regression at low quantities of TATP the LOD was calculated by having a 5 % or less of false positive/negative when detecting TATP. The calculations lead to a limit of detection of **0.12 mgL^{-1}**. (Same method than previous LODs).

Using less TATP leads to low repeatability because of the difficult when handling low quantities. Therefore, 0.12 mgL^{-1} represents the minimum amount reliably detected by the technique developed.

5.5. Summary of fluorescence measurements

- The presence of TATP may be detected easily and qualitatively with any of the silica systems with a code of colors or registering the increase in fluorescence.
- In order to distinguish with more precision, by registering the spectra and the increase in fluorescence, it is possible to distinguish selectively TATP from acid.

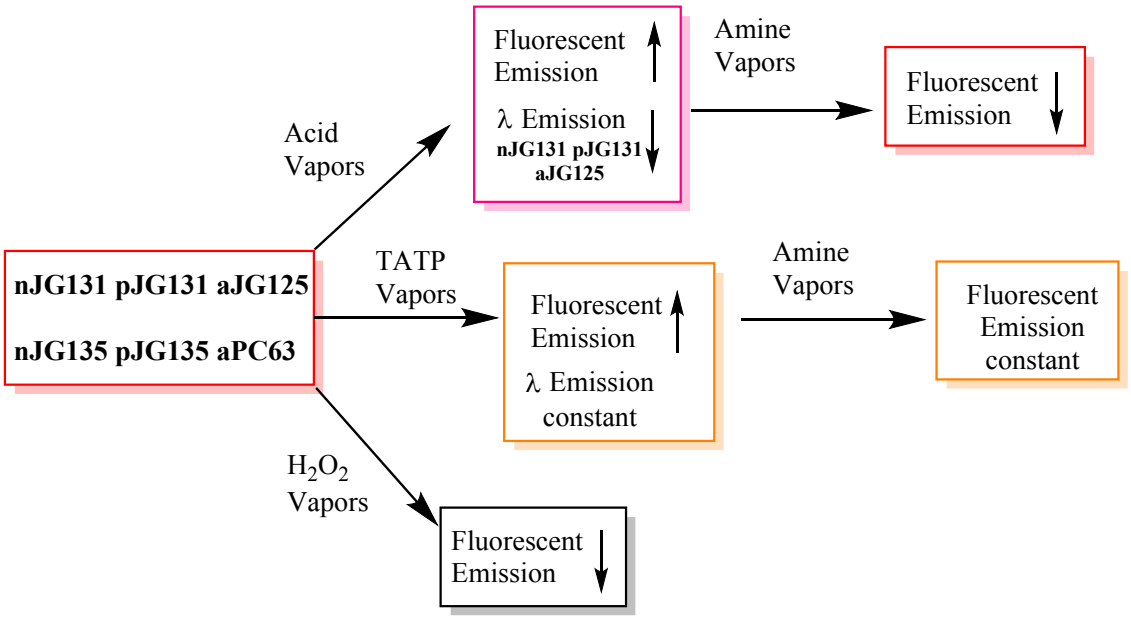

Figure S62. Scheme showing the interpretation of the results and the application of the different probes.

5.6. Electrochemistry

Cyclic voltammetry of compounds **JG125** and **JG125d.** Internal reference: Ferrocene

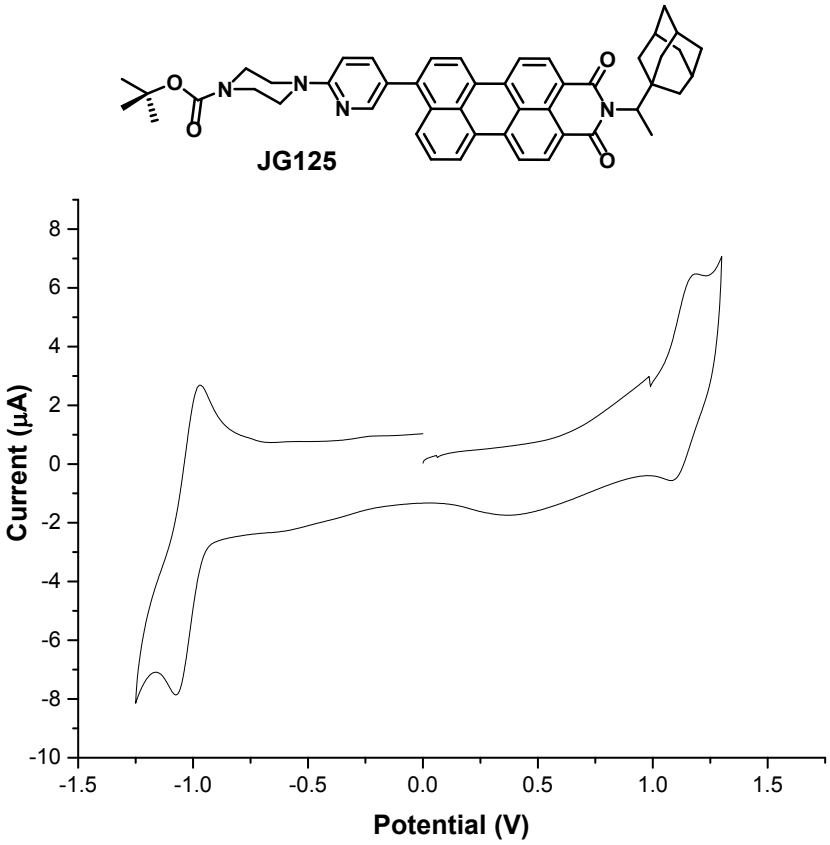

Figure S63. Cyclic voltammetry of compound JG125

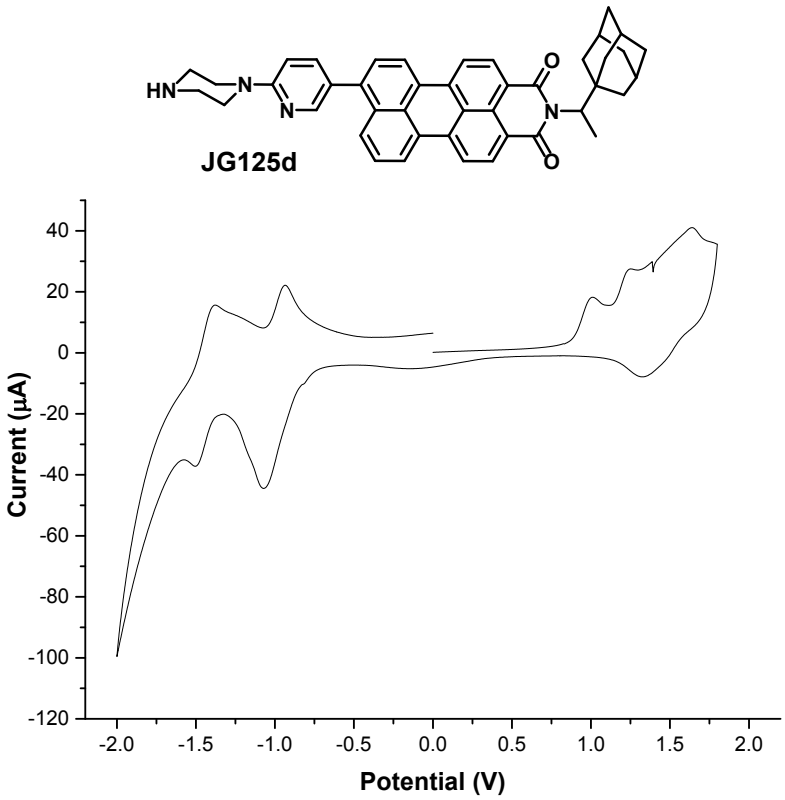

Figure S64. Cyclic voltammetry of compound JG125d

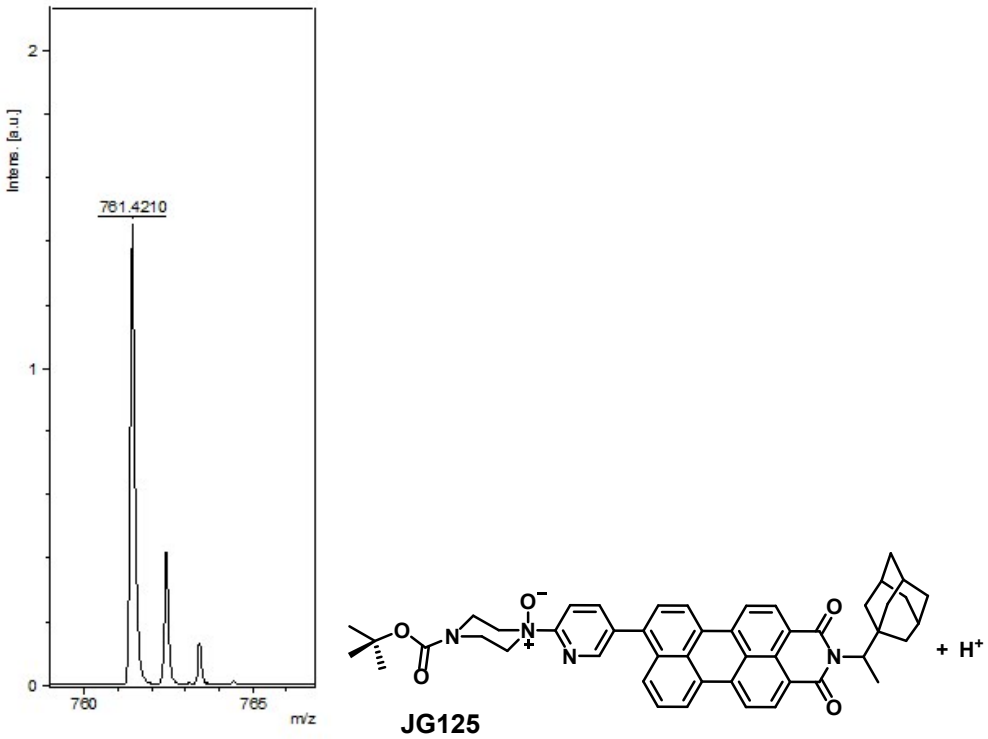

Figure S65. Mass spectrometry of compound JG125[O]. The highest peak corresponds to JG125 + Oxygen + H^+, detected by Mass Spectrometry in the MALDI MS spectrum. HRMS (MALDI) m/z calcd for $C_{48}H_{49}N_4O_5$: 761.3703 (M^++1); found: 761.4210.

5.7. Quantum chemical calculations

Table S01. Atomic coordinates of optimized **JG125**

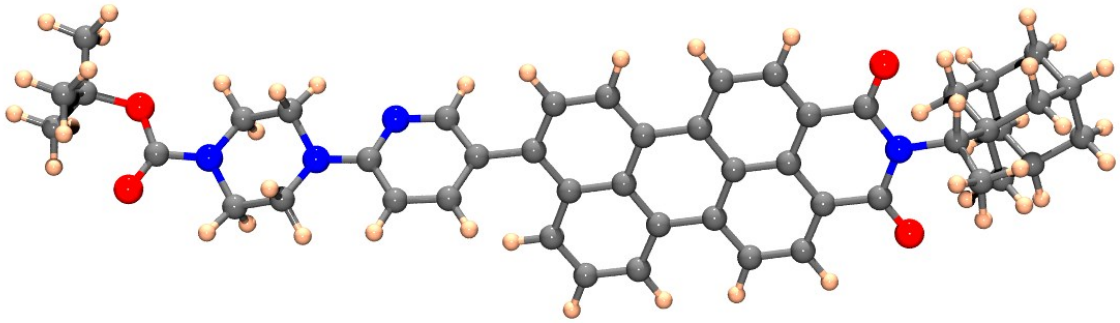

Center Number	Atomic Number	Atomic Type	Coordinates (Angstroms)		
			X	Y	Z
1	6	0	-0.847896	3.281212	1.010514
2	6	0	0.526673	3.121075	0.78561
3	6	0	1.042111	1.951191	0.232674
4	6	0	0.140825	0.891287	-0.114524
5	6	0	-1.274545	1.080423	0.061523
6	6	0	-1.731504	2.285349	0.655587

7	6	0	2.486173	1.777416	0.008493
8	6	0	0.635543	-0.355948	-0.614778
9	6	0	2.080643	-0.554114	-0.784121
10	6	0	2.9709	0.523976	-0.480716
11	6	0	2.626161	-1.759655	-1.239337
12	6	0	-0.284421	-1.354349	-0.923805
13	6	0	-1.663036	-1.156567	-0.79188
14	6	0	-2.189346	0.04049	-0.324964
15	1	0	-2.337484	-1.949819	-1.097487
16	1	0	-1.211569	4.193188	1.472934
17	1	0	-2.788809	2.411587	0.851682
18	6	0	3.411438	2.796857	0.255628
19	6	0	4.781239	2.614222	0.053607
20	6	0	5.275345	1.400744	-0.402484
21	6	0	4.376443	0.344783	-0.673866
22	1	0	5.477867	3.420675	0.252819
23	6	0	4.001389	-1.927351	-1.411917
24	1	0	4.398333	-2.871707	-1.766719
25	6	0	4.882592	-0.890318	-1.138575
26	1	0	1.982169	-2.598648	-1.47055
27	1	0	0.051661	-2.310757	-1.30527
28	1	0	1.188177	3.928385	1.074602
29	1	0	3.078361	3.764393	0.609033
30	6	0	-3.659972	0.193914	-0.249458
31	6	0	-4.457675	-0.807891	0.321086
32	6	0	-4.36219	1.282784	-0.801339
33	1	0	-3.982128	-1.682014	0.763949
34	6	0	-5.743807	1.335515	-0.748818
35	1	0	-3.822473	2.077334	-1.307362
36	6	0	-6.450021	0.278984	-0.121032
37	1	0	-6.257642	2.164769	-1.215987
38	7	0	-5.78815	-0.780189	0.389854
39	6	0	6.330393	-1.090763	-1.342418
40	6	0	6.731384	1.236597	-0.602351
41	8	0	6.7737	-2.163215	-1.752216
42	8	0	7.509278	2.162153	-0.378103
43	7	0	7.193223	-0.010252	-1.052663
44	6	0	8.65336	-0.234708	-1.33316
45	1	0	8.629121	-1.182447	-1.87082
46	6	0	9.199399	0.814013	-2.313185
47	1	0	8.527207	0.897966	-3.172982
48	1	0	9.305752	1.799645	-1.864646

49	1	0	10.171789	0.488687	-2.691893
50	6	0	9.533977	-0.522139	-0.067593
51	6	0	8.793793	-1.48222	0.901663
52	6	0	10.821043	-1.251424	-0.554947
53	6	0	9.971697	0.732061	0.732099
54	1	0	8.476125	-2.38134	0.359791
55	1	0	7.883835	-0.999007	1.277591
56	6	0	9.693908	-1.872408	2.09182
57	1	0	11.386168	-0.607604	-1.239337
58	1	0	10.540982	-2.15052	-1.120598
59	6	0	11.725153	-1.644717	0.630572
60	1	0	9.093428	1.268262	1.099082
61	1	0	10.509566	1.426968	0.076017
62	6	0	10.877634	0.339012	1.91853
63	1	0	9.134953	-2.544137	2.756078
64	6	0	10.955443	-2.59007	1.572754
65	6	0	10.106117	-0.603329	2.863865
66	1	0	12.618047	-2.153076	0.244439
67	6	0	12.140546	-0.375789	1.400572
68	1	0	11.166026	1.248751	2.460977
69	1	0	10.675597	-3.50849	1.040006
70	1	0	11.59458	-2.889887	2.413804
71	1	0	9.215555	-0.095523	3.257109
72	1	0	10.730113	-0.87102	3.726883
73	1	0	12.799516	-0.640141	2.238243
74	1	0	12.711163	0.294486	0.744013
75	6	0	-8.662077	1.312223	-0.583688
76	6	0	-8.526923	-0.992889	0.244274
77	6	0	-9.949178	1.511128	0.22303
78	1	0	-8.912345	1.050888	-1.624145
79	1	0	-8.129328	2.263157	-0.591486
80	6	0	-9.804525	-0.785363	1.055838
81	1	0	-8.785171	-1.447646	-0.725547
82	1	0	-7.854791	-1.668161	0.769821
83	1	0	-10.622593	2.185375	-0.304531
84	1	0	-9.697477	1.957487	1.195757
85	1	0	-10.36213	-1.717628	1.109914
86	1	0	-9.544474	-0.474312	2.077806
87	7	0	-7.826844	0.277688	0.024032
88	7	0	-10.634496	0.24314	0.433108
89	6	0	-11.980759	0.148016	0.203678
90	8	0	-12.655857	1.06558	-0.254177

91	8	0	-12.447589	-1.077213	0.535666
92	6	0	-13.864524	-1.441862	0.342314
93	6	0	-14.758098	-0.552761	1.211917
94	6	0	-14.229186	-1.365221	-1.142948
95	6	0	-13.9005	-2.890903	0.833839
96	1	0	-14.439818	-0.601762	2.257942
97	1	0	-14.722685	0.484372	0.878832
98	1	0	-15.791881	-0.907496	1.154573
99	1	0	-13.542161	-1.977873	-1.735041
100	1	0	-15.242229	-1.752556	-1.290066
101	1	0	-14.189137	-0.337662	-1.504032
102	1	0	-14.914508	-3.290639	0.744554
103	1	0	-13.22832	-3.517356	0.240293
104	1	0	-13.596189	-2.951374	1.882754

Table S02. Atomic coordinates of optimized oxidized **JG125**$^{+\cdot}$.

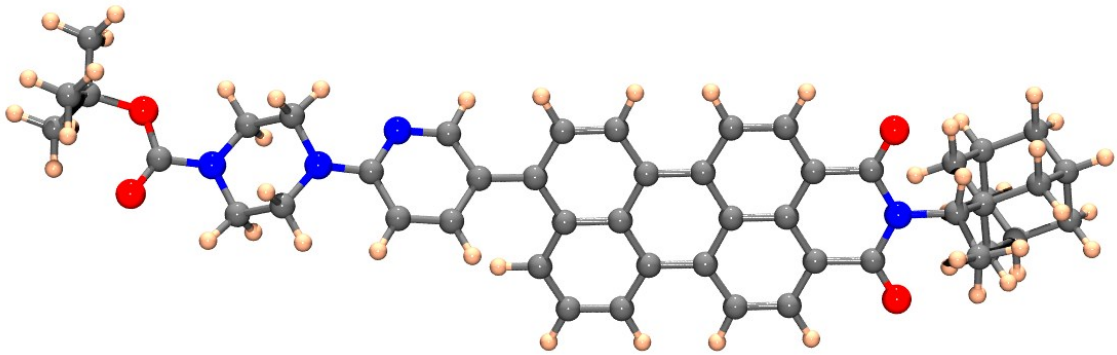

Center Number	Atomic Number	Atomic Type	Coordinates (Angstroms)		
			X	Y	Z
1	6	0	-0.942018	3.216026	1.022741
2	6	0	0.425057	3.085892	0.792945
3	6	0	0.969726	1.894975	0.29146
4	6	0	0.090631	0.805958	-0.006869
5	6	0	-1.327645	0.972485	0.157766
6	6	0	-1.806792	2.175462	0.717032
7	6	0	2.409093	1.738796	0.084125
8	6	0	0.614449	-0.456254	-0.432548
9	6	0	2.043952	-0.617485	-0.636649
10	6	0	2.912239	0.488129	-0.37912
11	6	0	2.609719	-1.82305	-1.092193
12	6	0	-0.285831	-1.522911	-0.626595
13	6	0	-1.65171	-1.359183	-0.497798
14	6	0	-2.221977	-0.111675	-0.178884
15	1	0	-2.297755	-2.196631	-0.734637

16	1	0	-1.329977	4.132332	1.454042
17	1	0	-2.859171	2.280033	0.947583
18	6	0	3.322344	2.780389	0.314514
19	6	0	4.691793	2.620366	0.102044
20	6	0	5.1976	1.40848	-0.349594
21	6	0	4.314811	0.334953	-0.592508
22	1	0	5.3766	3.439868	0.285026
23	6	0	3.981426	-1.959819	-1.295555
24	1	0	4.395234	-2.895713	-1.651409
25	6	0	4.838587	-0.893411	-1.050697
26	1	0	1.981189	-2.677605	-1.305519
27	1	0	0.078995	-2.498454	-0.919323
28	1	0	1.067507	3.921355	1.03903
29	1	0	2.976509	3.745398	0.661176
30	6	0	-3.663298	0.032449	-0.262795
31	6	0	-4.52198	-1.036634	0.113243
32	6	0	-4.318122	1.182842	-0.773329
33	1	0	-4.093691	-1.942931	0.535621
34	6	0	-5.686838	1.225763	-0.877906
35	1	0	-3.736664	2.018464	-1.145291
36	6	0	-6.453261	0.102032	-0.443295
37	1	0	-6.152018	2.093045	-1.324631
38	7	0	-5.836637	-1.007519	0.048611
39	6	0	6.294552	-1.061841	-1.29186
40	6	0	6.660593	1.267774	-0.572076
41	8	0	6.734421	-2.126985	-1.712819
42	8	0	7.413198	2.211946	-0.360723
43	7	0	7.139905	0.031614	-1.026249
44	6	0	8.600623	-0.159819	-1.347698
45	1	0	8.58168	-1.098974	-1.900506
46	6	0	9.098374	0.916084	-2.323664
47	1	0	8.38675	1.024329	-3.147999
48	1	0	9.231175	1.889351	-1.855547
49	1	0	10.049811	0.598077	-2.756653
50	6	0	9.512083	-0.446208	-0.105271
51	6	0	8.832246	-1.472398	0.840456
52	6	0	10.824736	-1.095719	-0.634495
53	6	0	9.900406	0.80076	0.730366
54	1	0	8.550761	-2.36846	0.274177
55	1	0	7.906117	-1.045804	1.245254
56	6	0	9.767018	-1.858032	2.005188
57	1	0	11.349835	-0.400658	-1.29992

58	1	0	10.580502	-1.985559	-1.230519
59	6	0	11.762283	-1.486236	0.525716
60	1	0	9.00386	1.280936	1.130609
61	1	0	10.393814	1.543166	0.09198
62	6	0	10.842005	0.411936	1.89055
63	1	0	9.249105	-2.576547	2.653357
64	6	0	11.052245	-2.49818	1.445554
65	6	0	10.130414	-0.597069	2.813833
66	1	0	12.671918	-1.938151	0.110158
67	6	0	12.129022	-0.224935	1.331886
68	1	0	11.095075	1.316172	2.458798
69	1	0	10.807749	-3.410796	0.886203
70	1	0	11.717267	-2.794546	2.267247
71	1	0	9.223123	-0.14605	3.237153
72	1	0	10.779623	-0.863381	3.658196
73	1	0	12.81148	-0.484975	2.151658
74	1	0	12.658092	0.49245	0.690757
75	6	0	-8.65404	1.15822	-0.986976
76	6	0	-8.570715	-1.144422	-0.14431
77	6	0	-9.735632	1.492651	0.054029
78	1	0	-9.129263	0.846242	-1.924748
79	1	0	-8.061232	2.047635	-1.182369
80	6	0	-9.649964	-0.805586	0.894175
81	1	0	-9.047579	-1.531577	-1.053169
82	1	0	-7.880446	-1.88943	0.242187
83	1	0	-10.432053	2.221107	-0.358928
84	1	0	-9.25787	1.923745	0.943516
85	1	0	-10.2714	-1.680365	1.069787
86	1	0	-9.167826	-0.524686	1.83979
87	7	0	-7.808546	0.059113	-0.510128
88	7	0	-10.477153	0.298541	0.424257
89	6	0	-11.839732	0.256318	0.247967
90	8	0	-12.488334	1.202513	-0.18443
91	8	0	-12.3395	-0.940407	0.616173
92	6	0	-13.787975	-1.23209	0.539412
93	6	0	-14.558563	-0.288372	1.466211
94	6	0	-14.26288	-1.146978	-0.913474
95	6	0	-13.85852	-2.672887	1.049386
96	1	0	-14.16621	-0.351898	2.485841
97	1	0	-14.489858	0.743895	1.122776
98	1	0	-15.612348	-0.582519	1.488777
99	1	0	-13.659507	-1.801261	-1.550391

100	1	0	-15.30353	-1.479937	-0.974599
101	1	0	-14.198337	-0.126276	-1.290213
102	1	0	-14.895495	-3.01981	1.041781
103	1	0	-13.267112	-3.337814	0.41329
104	1	0	-13.478875	-2.740854	2.072901}

Table S03. Atomic coordinates of optimized **JG125d**

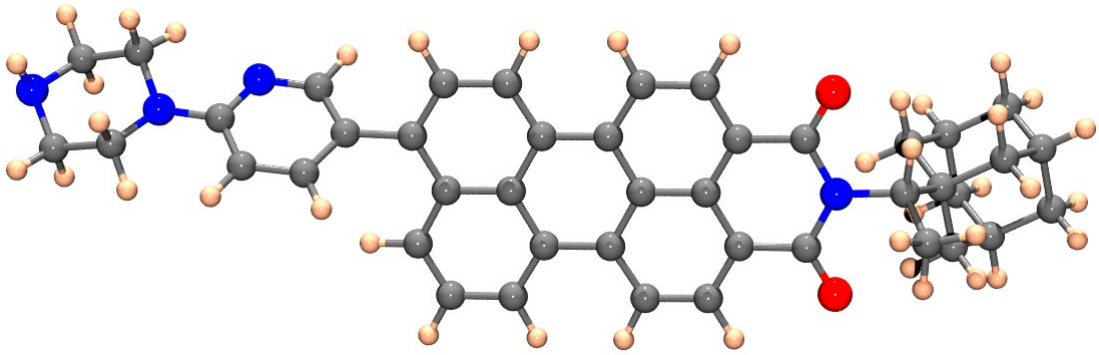

Center Number	Atomic Number	Atomic Type	Coordinates (Angstroms)		
			X	Y	Z
1	6	0	-3.165173	3.073938	0.799233
2	6	0	-1.783353	2.975156	0.584225
3	6	0	-1.198952	1.794018	0.13277
4	6	0	-2.03789	0.661094	-0.130621
5	6	0	-3.460527	0.776879	0.050435
6	6	0	-3.987783	1.998873	0.542123
7	6	0	0.255176	1.681979	-0.065305
8	6	0	-1.473462	-0.58603	-0.55116
9	6	0	-0.023609	-0.701598	-0.751896
10	6	0	0.806791	0.436516	-0.501744
11	6	0	0.583203	-1.886272	-1.184047
12	6	0	-2.331535	-1.664028	-0.752702
13	6	0	-3.717072	-1.545784	-0.59914
14	6	0	-4.31205	-0.34848	-0.224996
15	1	0	-4.343717	-2.405282	-0.814142
16	1	0	-3.582317	4.000971	1.179246
17	1	0	-5.050312	2.077532	0.735281
18	6	0	1.127343	2.752969	0.156658
19	6	0	2.506174	2.632252	-0.029169
20	6	0	3.063075	1.433406	-0.450205
21	6	0	2.219558	0.326168	-0.694371
22	1	0	3.160818	3.476901	0.153405
23	6	0	1.963317	-1.981649	-1.370407

24	1	0	2.408507	-2.91059	-1.708252
25	6	0	2.788803	-0.891988	-1.129862
26	1	0	-0.015776	-2.76455	-1.388779
27	1	0	-1.940486	-2.626648	-1.058697
28	1	0	-1.171606	3.843116	0.796827
29	1	0	0.745152	3.712243	0.481644
30	6	0	-5.787619	-0.284539	-0.121296
31	6	0	-6.500427	-1.264938	0.58242
32	6	0	-6.576357	0.687761	-0.766438
33	1	0	-5.9545	-2.050707	1.103278
34	6	0	-7.956169	0.654466	-0.677061
35	1	0	-6.104406	1.456344	-1.371107
36	6	0	-8.575103	-0.368603	0.087053
37	1	0	-8.536198	1.392614	-1.214066
38	7	0	-7.827549	-1.317077	0.691311
39	6	0	4.243221	-1.018727	-1.342838
40	6	0	4.527178	1.335006	-0.633013
41	8	0	4.740069	-2.073044	-1.738363
42	8	0	5.260656	2.29481	-0.402218
43	7	0	5.049387	0.110361	-1.077112
44	6	0	6.517525	-0.042831	-1.360717
45	1	0	6.538146	-0.993826	-1.892272
46	6	0	7.008938	1.024748	-2.348631
47	1	0	6.348215	1.050651	-3.221024
48	1	0	7.042563	2.021703	-1.913896
49	1	0	8.007869	0.759318	-2.704829
50	6	0	7.417742	-0.277513	-0.09672
51	6	0	6.702052	-1.206517	0.919273
52	6	0	8.702214	-1.014858	-0.578492
53	6	0	7.858628	1.009544	0.647067
54	1	0	6.38345	-2.127922	0.416934
55	1	0	5.794627	-0.717207	1.29325
56	6	0	7.625556	-1.545303	2.107539
57	1	0	9.248554	-0.394209	-1.299068
58	1	0	8.4193	-1.937811	-1.10257
59	6	0	9.630278	-1.355523	0.604336
60	1	0	6.981146	1.552681	1.005913
61	1	0	8.380707	1.681601	-0.045005
62	6	0	8.787356	0.667792	1.832126
63	1	0	7.083542	-2.196196	2.805686
64	6	0	8.884613	-2.27138	1.594148
65	6	0	8.03975	-0.245118	2.824652

66	1	0	10.520865	-1.870958	0.222257
67	6	0	10.047732	-0.055879	1.319929
68	1	0	9.076899	1.599225	2.335759
69	1	0	8.604042	-3.211217	1.100579
70	1	0	9.540327	-2.534187	2.434749
71	1	0	7.151901	0.26996	3.214484
72	1	0	8.680974	-0.475302	3.685884
73	1	0	10.721624	-0.284527	2.156275
74	1	0	10.602602	0.593831	0.630094
75	6	0	-10.858731	0.427511	-0.466866
76	6	0	-10.542084	-1.706969	0.721496
77	6	0	-12.176609	0.614548	0.302963
78	1	0	-11.065794	0.008248	-1.466339
79	1	0	-10.405167	1.40965	-0.607365
80	6	0	-11.852111	-1.454914	1.473515
81	1	0	-10.739124	-2.352957	-0.151587
82	1	0	-9.821293	-2.220672	1.355498
83	1	0	-12.87446	1.180795	-0.322355
84	1	0	-11.976731	1.214108	1.200238
85	1	0	-12.316364	-2.41561	1.719176
86	1	0	-11.631423	-0.943032	2.418938
87	7	0	-9.942993	-0.442115	0.273253
88	7	0	-12.813027	-0.631965	0.731125
89	1	0	-13.116334	-1.147726	-0.095

Table S04. Atomic coordinates of optimized oxidized **JG125d**$^{+\cdot}$.

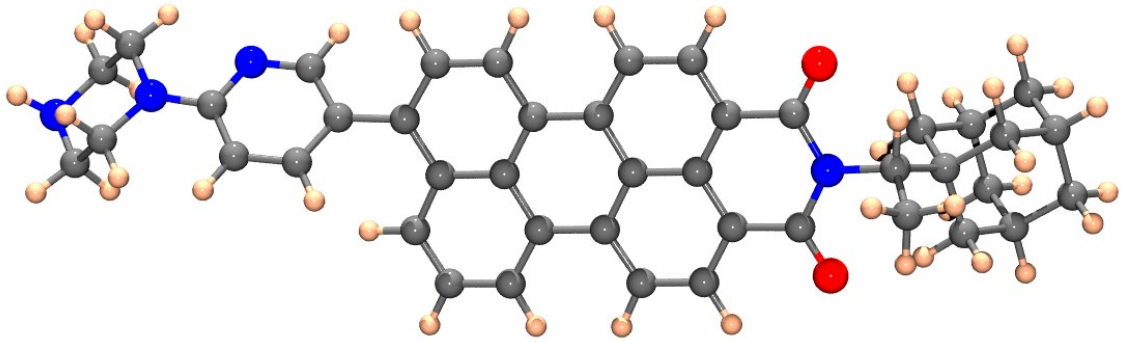

Center Number	Atomic Number	Atomic Type	Coordinates (Angstroms)		
			X	Y	Z
1	6	0	-3.239971	3.050656	0.656458
2	6	0	-1.865885	2.948785	0.439422
3	6	0	-1.2697	1.726804	0.109559
4	6	0	-2.099365	0.567728	-0.02693
5	6	0	-3.52355	0.691852	0.126528

6	6	0	-4.056469	1.942275	0.509722
7	6	0	0.178472	1.607613	-0.082848
8	6	0	-1.519816	-0.71709	-0.280259
9	6	0	-0.080385	-0.839786	-0.475745
10	6	0	0.737227	0.328541	-0.37706
11	6	0	0.536705	-2.066577	-0.769531
12	6	0	-2.367578	-1.836278	-0.319408
13	6	0	-3.742695	-1.717596	-0.198078
14	6	0	-4.365752	-0.469539	-0.039616
15	1	0	-4.350105	-2.608331	-0.311616
16	1	0	-3.667493	4.002357	0.953151
17	1	0	-5.112882	2.032728	0.72733
18	6	0	1.042889	2.708009	0.001881
19	6	0	2.419442	2.581707	-0.194846
20	6	0	2.979311	1.346182	-0.487082
21	6	0	2.145217	0.211171	-0.580395
22	1	0	3.066574	3.44812	-0.124875
23	6	0	1.913841	-2.168226	-0.96683
24	1	0	2.367966	-3.124233	-1.198805
25	6	0	2.722447	-1.042965	-0.877341
26	1	0	-0.05273	-2.969533	-0.860182
27	1	0	-1.960559	-2.825629	-0.481125
28	1	0	-1.261984	3.838926	0.55923
29	1	0	0.654938	3.694565	0.219595
30	6	0	-5.818061	-0.406928	-0.108362
31	6	0	-6.61524	-1.442692	0.452003
32	6	0	-6.535208	0.614286	-0.779693
33	1	0	-6.133707	-2.254451	0.992748
34	6	0	-7.907745	0.577566	-0.85394
35	1	0	-6.001777	1.4073	-1.290643
36	6	0	-8.606993	-0.491411	-0.220335
37	1	0	-8.425291	1.342956	-1.414889
38	7	0	-7.930904	-1.483689	0.418295
39	6	0	4.180685	-1.174777	-1.117602
40	6	0	4.444982	1.242305	-0.700426
41	8	0	4.671363	-2.265816	-1.393517
42	8	0	5.162164	2.231912	-0.596826
43	7	0	4.972663	-0.014213	-1.027302
44	6	0	6.428582	-0.171751	-1.381291
45	1	0	6.442072	-1.179614	-1.794391
46	6	0	6.819449	0.77973	-2.520858
47	1	0	6.113383	0.67171	-3.350174

48	1	0	6.836352	1.824405	-2.215924
49	1	0	7.808603	0.507631	-2.897905
50	6	0	7.414303	-0.232491	-0.162081
51	6	0	6.78465	-1.022537	1.014394
52	6	0	8.670188	-1.022172	-0.638146
53	6	0	7.892716	1.142414	0.372086
54	1	0	6.440372	-2.001954	0.660414
55	1	0	5.902406	-0.489045	1.388746
56	6	0	7.796848	-1.202591	2.165095
57	1	0	9.153473	-0.498387	-1.471646
58	1	0	8.363162	-2.007092	-1.014974
59	6	0	9.685784	-1.202698	0.507435
60	1	0	7.03757	1.727081	0.719718
61	1	0	8.358769	1.718108	-0.436851
62	6	0	8.908133	0.959735	1.521175
63	1	0	7.315132	-1.758907	2.97941
64	6	0	9.024488	-1.98537	1.657731
65	6	0	8.246012	0.181112	2.67511
66	1	0	10.552283	-1.760838	0.130459
67	6	0	10.137507	0.180113	1.015415
68	1	0	9.22099	1.949636	1.877489
69	1	0	8.720394	-2.981533	1.310252
70	1	0	9.741704	-2.136171	2.47508
71	1	0	7.38312	0.740184	3.060291
72	1	0	8.951435	0.065944	3.508592
73	1	0	10.873375	0.065156	1.822083
74	1	0	10.631887	0.736038	0.207765
75	6	0	-10.874022	0.416719	-0.75805
76	6	0	-10.668219	-1.681369	0.462093
77	6	0	-11.716042	1.003643	0.409892
78	1	0	-11.539348	-0.063916	-1.483959
79	1	0	-10.332741	1.210127	-1.266806
80	6	0	-11.510125	-1.080409	1.618944
81	1	0	-11.331497	-2.170944	-0.260143
82	1	0	-9.94126	-2.399365	0.832023
83	1	0	-12.444942	1.705911	-0.003134
84	1	0	-11.042521	1.56329	1.069922
85	1	0	-12.093136	-1.881065	2.081754
86	1	0	-10.822205	-0.683735	2.375071
87	7	0	-9.964035	-0.600993	-0.235953
88	7	0	-12.401132	-0.014599	1.186926
89	1	0	-13.188486	-0.393906	0.666747

HOMO
JG125d

SOMO
[JG125d]$^{+}$

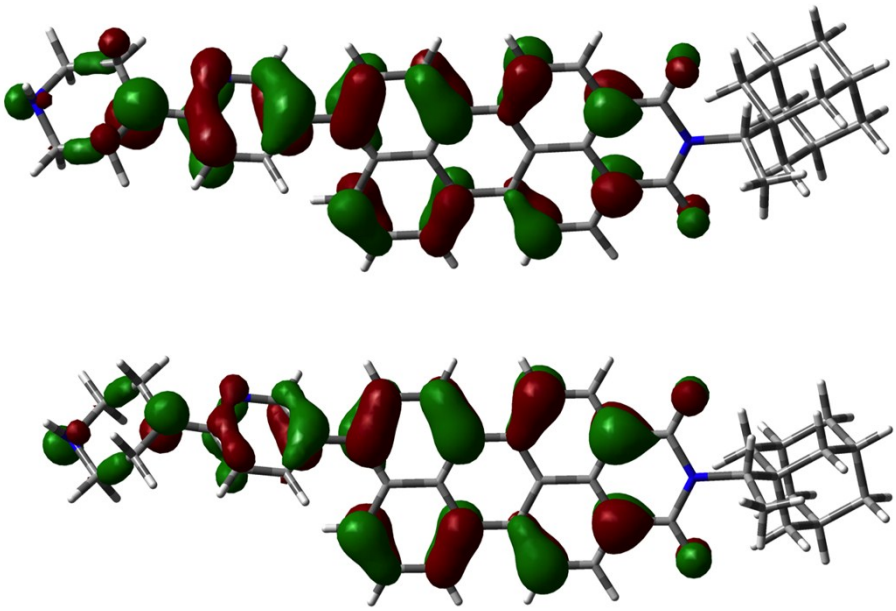

Figure S66. DFT calculated HOMO and SOMO plots for compound JG125d.

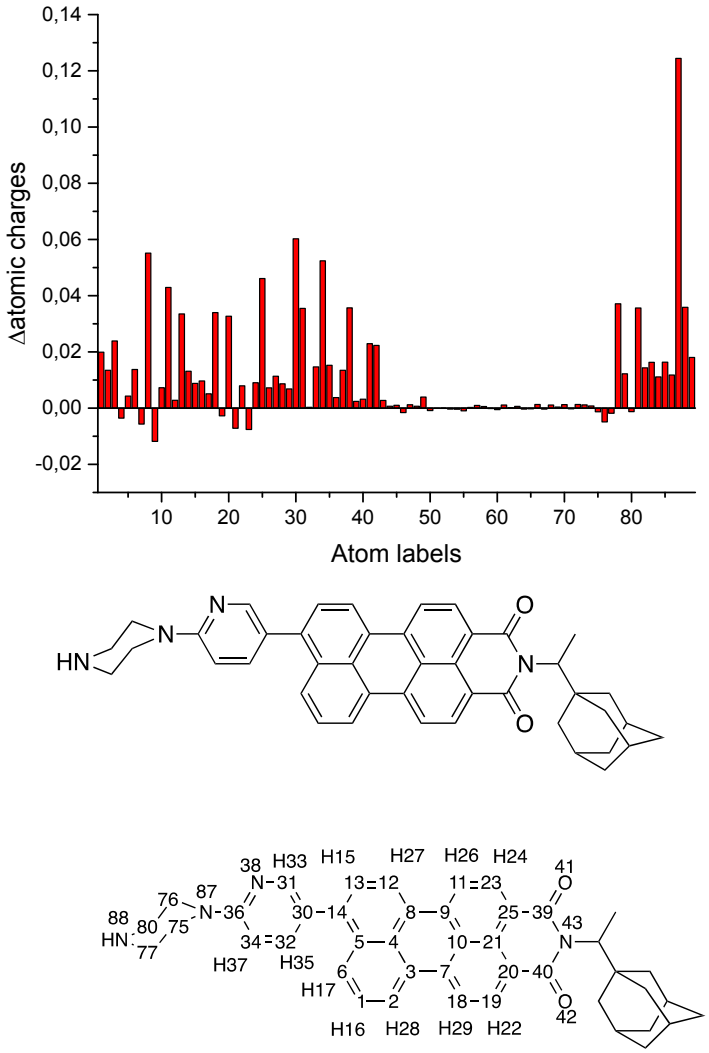

Figure S67. Difference between the charges of the atoms in JGC125d and the cationic radical JG125d^{+}. The higher variation is observed for the nitrogen atom labeled as 87.

Table S05. Atomic coordinates of optimized *N*-oxide **JC125[O].**

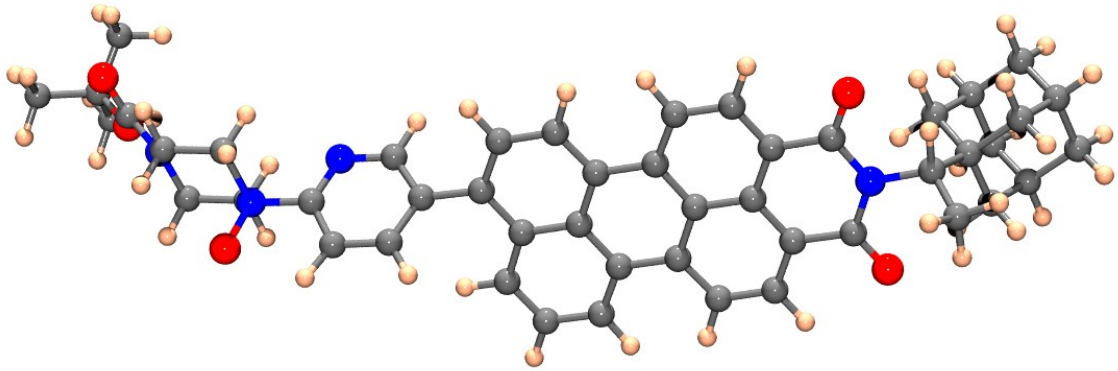

Center Number	Atomic Number	Atomic Type	Coordinates (Angstroms)		
			X	Y	Z
1	6	0	-0.762971	2.793887	2.339057
2	6	0	0.617508	2.662447	2.12898
3	6	0	1.125404	1.927084	1.061283
4	6	0	0.209597	1.298199	0.154495
5	6	0	-1.205507	1.466612	0.349496
6	6	0	-1.658238	2.209013	1.471223
7	6	0	2.574581	1.772962	0.852313
8	6	0	0.687404	0.493348	-0.929891
9	6	0	2.133839	0.319914	-1.128605
10	6	0	3.041735	0.966001	-0.232138
11	6	0	2.660098	-0.454946	-2.166597
12	6	0	-0.244463	-0.113198	-1.765992
13	6	0	-1.622065	0.065936	-1.589055
14	6	0	-2.124898	0.853093	-0.56566
15	1	0	-2.306745	-0.400884	-2.289794
16	1	0	-1.122025	3.354815	3.195801
17	1	0	-2.721463	2.301228	1.655299
18	6	0	3.520789	2.387441	1.67791
19	6	0	4.893821	2.222182	1.477583
20	6	0	5.368905	1.434617	0.439823
21	6	0	4.448602	0.801894	-0.426095
22	1	0	5.606447	2.707293	2.134871
23	6	0	4.036685	-0.613515	-2.342849
24	1	0	4.419724	-1.221245	-3.154619
25	6	0	4.935674	0.003383	-1.485369
26	1	0	2.001607	-0.955465	-2.86509
27	1	0	0.079157	-0.733435	-2.592447
28	1	0	1.286954	3.138664	2.834427
29	1	0	3.204402	3.014058	2.502027

30	6	0	-3.597021	1.026711	-0.462087
31	6	0	-4.436173	-0.099302	-0.429017
32	6	0	-4.221241	2.284389	-0.455141
33	1	0	-4.005655	-1.097557	-0.422829
34	6	0	-5.610334	2.372025	-0.412238
35	1	0	-3.623373	3.188891	-0.501539
36	6	0	-6.317394	1.178172	-0.384103
37	1	0	-6.15722	3.303994	-0.410521
38	7	0	-5.771452	-0.029656	-0.392424
39	6	0	6.385913	-0.18317	-1.693608
40	6	0	6.828355	1.268012	0.260151
41	8	0	6.810828	-0.875877	-2.61723
42	8	0	7.625827	1.818943	1.016208
43	7	0	7.26867	0.455356	-0.79577
44	6	0	8.735801	0.265098	-1.062577
45	1	0	8.718294	-0.216923	-2.039526
46	6	0	9.449792	1.611244	-1.249313
47	1	0	8.904133	2.218768	-1.97828
48	1	0	9.53584	2.179044	-0.325032
49	1	0	10.45095	1.439309	-1.653548
50	6	0	9.449129	-0.77136	-0.124635
51	6	0	8.522024	-1.984107	0.153453
52	6	0	10.695581	-1.304029	-0.892168
53	6	0	9.935857	-0.206836	1.235137
54	1	0	8.16816	-2.404238	-0.796069
55	1	0	7.634413	-1.654772	0.706962
56	6	0	9.254962	-3.068602	0.970094
57	1	0	11.387722	-0.480885	-1.107355
58	1	0	10.381302	-1.717476	-1.860088
59	6	0	11.433085	-2.388378	-0.080987
60	1	0	9.087724	0.175627	1.807756
61	1	0	10.608834	0.643176	1.067997
62	6	0	10.673345	-1.293302	2.047615
63	1	0	8.566225	-3.90359	1.152397
64	6	0	10.480765	-3.570642	0.182088
65	6	0	9.718565	-2.474053	2.314583
66	1	0	12.301742	-2.734077	-0.656059
67	6	0	11.900701	-1.793462	1.261532
68	1	0	10.99924	-0.861359	3.002737
69	1	0	10.161648	-4.017559	-0.768744
70	1	0	10.999529	-4.355934	0.747558
71	1	0	8.851144	-2.13251	2.894672

72	1	0	10.223406	-3.242826	2.914514
73	1	0	12.442648	-2.551273	1.842699
74	1	0	12.598956	-0.964772	1.083979
75	6	0	-8.354905	0.523519	-1.594145
76	6	0	-8.305154	0.477522	0.886285
77	6	0	-9.874893	0.507433	-1.551689
78	1	0	-7.934025	-0.483027	-1.624294
79	1	0	-7.992621	1.111966	-2.43801
80	6	0	-9.827157	0.458852	0.906417
81	1	0	-7.88301	-0.528458	0.863766
82	1	0	-7.911392	1.035508	1.736768
83	1	0	-10.261029	-0.050819	-2.403597
84	1	0	-10.239202	1.538746	-1.598563
85	1	0	-10.166206	-0.123289	1.760288
86	1	0	-10.188643	1.487605	1.00523
87	7	0	-7.820136	1.234457	-0.349689
88	7	0	-10.342677	-0.133107	-0.326318
89	6	0	-11.299596	-1.110385	-0.393683
90	8	0	-11.754304	-1.538999	-1.450242
91	8	0	-11.657231	-1.531055	0.84066
92	6	0	-12.664852	-2.592812	1.030968
93	6	0	-14.016909	-2.135922	0.475473
94	6	0	-12.178989	-3.898523	0.394931
95	6	0	-12.723234	-2.722848	2.554736
96	1	0	-14.310316	-1.183553	0.927849
97	1	0	-13.976552	-2.016708	-0.607107
98	1	0	-14.782097	-2.878728	0.721394
99	1	0	-11.190617	-4.164814	0.7824
100	1	0	-12.871716	-4.707126	0.648048
101	1	0	-12.122264	-3.810119	-0.689895
102	1	0	-13.44913	-3.491288	2.835115
103	1	0	-11.746543	-3.006469	2.957453
104	1	0	-13.026902	-1.77692	3.012407
105	8	0	-8.276047	2.515794	-0.315634

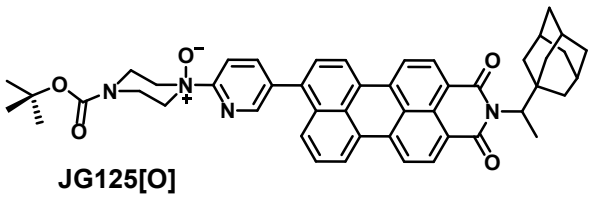

JG125[O]

HOMO
JG125[O]

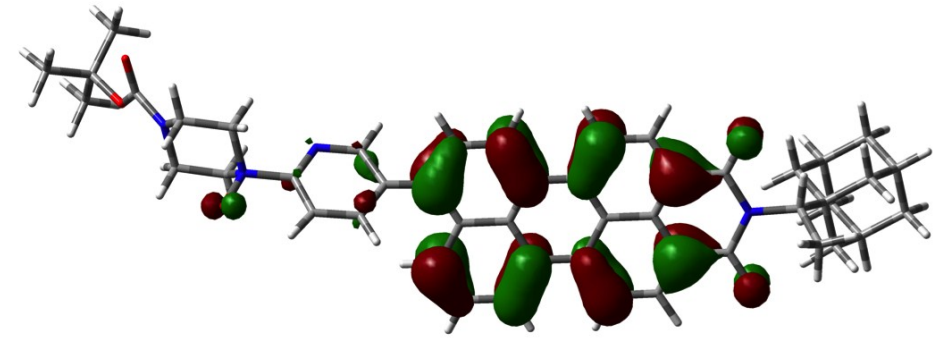

LUMO
JG125[O]

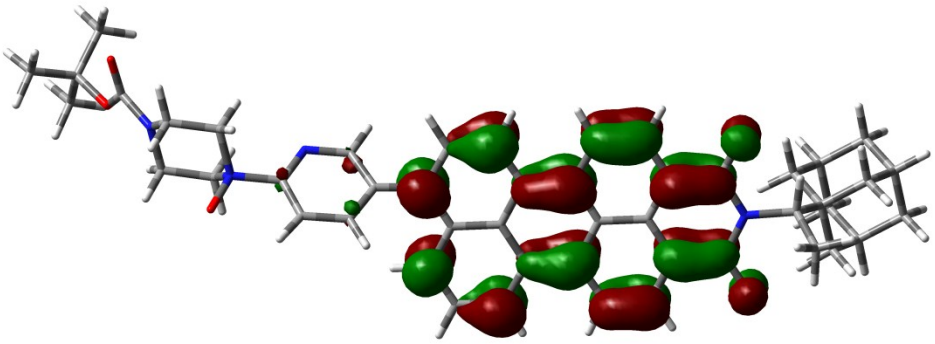

Figure S68. DFT calculated HOMO/LUMO plots for compound **JG125[O]**.